nature research

https://doi.org/10.1038/s41565-020-00782-3

Supplementary information

Proton-driven transformable nanovaccine for cancer immunotherapy

In the format provided by the authors and unedited

Supplementary Information

Proton-driven transformable nanovaccine for cancer immunotherapy

Ningqiang Gong[1,2,3,4], Yuxuan Zhang[2,4], Xucong Teng[1], Yongchao Wang[2], Shuaidong Huo[2,5], Guangchao Qing[2], Qiankun Ni[1,2,4], Xianlei Li[2,4], Jinjin Wang[2,4], Xiaoxia Ye[2], Tingbin Zhang[2], Shizhu Chen[2,6], Yongji Wang[1], Jie Yu[7], Paul C. Wang[2,8,9], Yaling Gan[2], Jinchao Zhang[6], Michael J. Mitchell[3], Jinghong Li[1,*] and Xing-Jie Liang[2,4,6,*]

Table of contents

Supplementary Figures

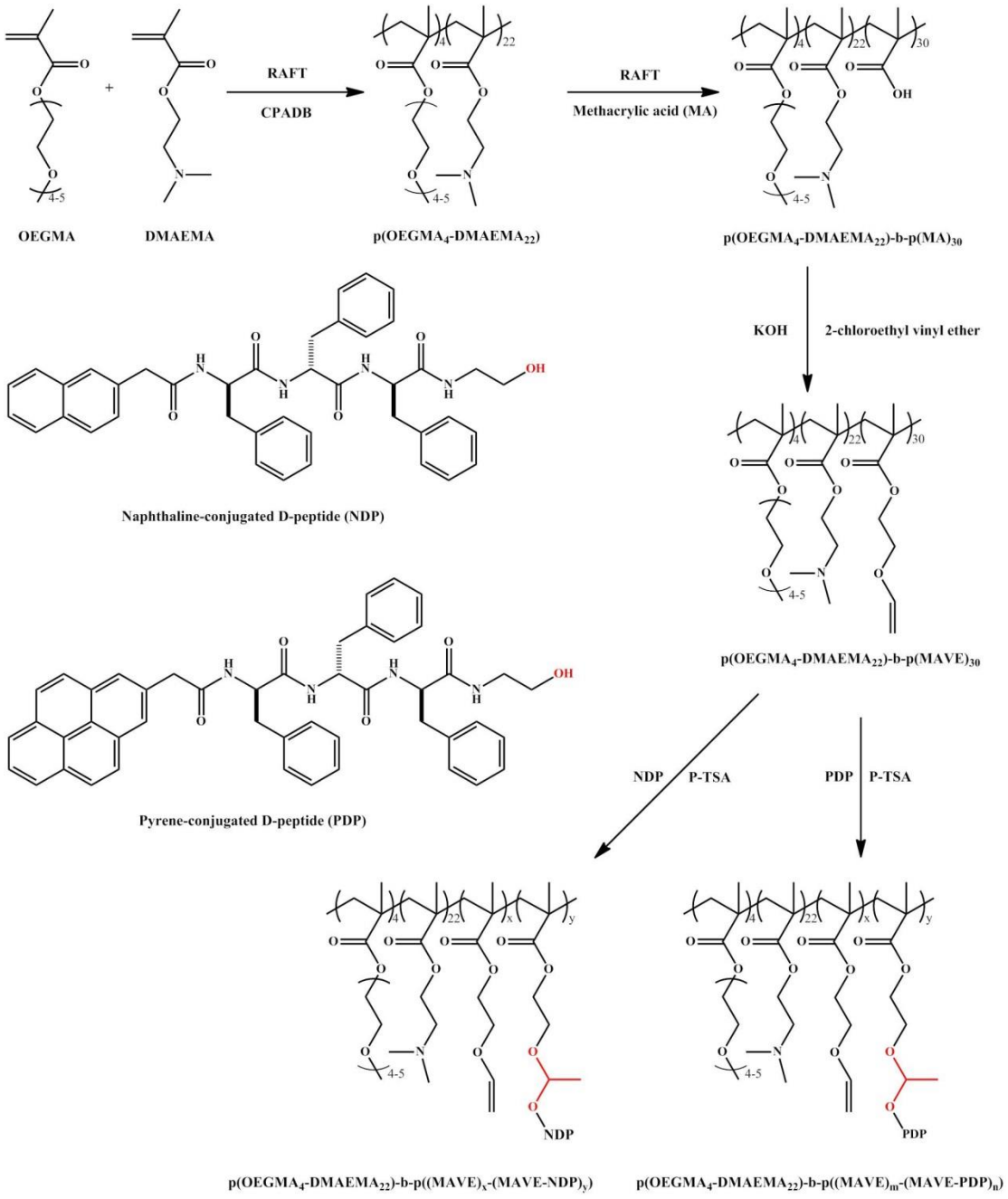

Supplementary Figure 1. Schematic syntheses of nanotransformers. p(OEGMA$_4$-DMAEMA$_{22}$) was first synthesized using a RAFT polymerization method. Next, p(OEGMA$_4$-DMAEMA$_{22}$) was used as a macroCTA to synthesize p(OEGMA$_4$-DMAEMA$_{22}$)-*b*-p(MA)$_{30}$ using the RAFT method. A vinyl ether of p(OEGMA$_4$-DMAEMA$_{22}$)-*b*-p(MA)$_{30}$ was then obtained by a reaction between 2-chloroethyl vinyl ether and the carboxyl group of p(OEGMA$_4$-DMAEMA$_{22}$)-*b*-p(MA)$_{30}$.

After that, naphthalene-conjugated D-peptide (NDP) or pyrene-conjugated D-peptide (PDP) was conjugated to p(OEGMA$_4$-DMAEMA$_{22}$)-*b*-p(MAVE)$_{30}$ through a pH-sensitive acetal bond. Finally, two kinds of nanotransformer that represent the “nanosphere to nanofiber” type (p(OEGMA$_4$-DMAEMA$_{22}$)-*b*-p((MAVE)$_x$-(MAVE-NDP)$_y$)) or the “nanosphere to nanosheet” type (p(OEGMA$_4$-DMAEMA$_{22}$)-*b*-p((MAVE)$_m$-(MAVE-PDP)$_n$)) were obtained, where x + y= 30, m + n = 30.

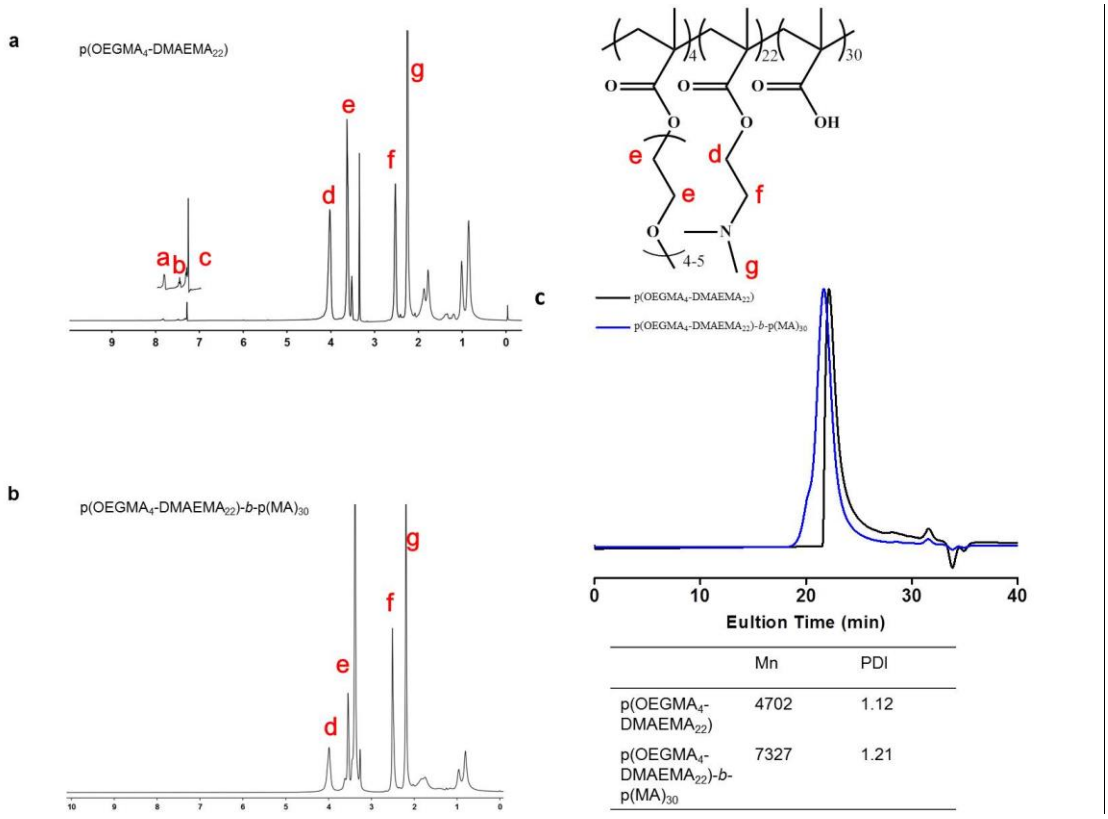

	Mn	PDI
p(OEGMA$_4$-DMAEMA$_{22}$)	4702	1.12
p(OEGMA$_4$-DMAEMA$_{22}$)-*b*-p(MA)$_{30}$	7327	1.21

Supplementary Figure 2. Syntheses and characterization of p(OEGMA$_4$-DMAEMA$_{22}$) and p(OEGMA$_4$-DMAEMA$_{22}$)-*b*-p(MA)$_{30}$. ^{1}H-NMR spectra (**a**), (**b**) and GPC traces (**c**) of as prepared p(OEGMA$_4$-DMAEMA$_{22}$) and p(OEGMA$_4$-DMAEMA$_{22}$)-*b*-p(MA)$_{30}$, respectively. The red characters a, b and c in (**a**) are the aromatic protons on the chain transfer agent (CPADB).

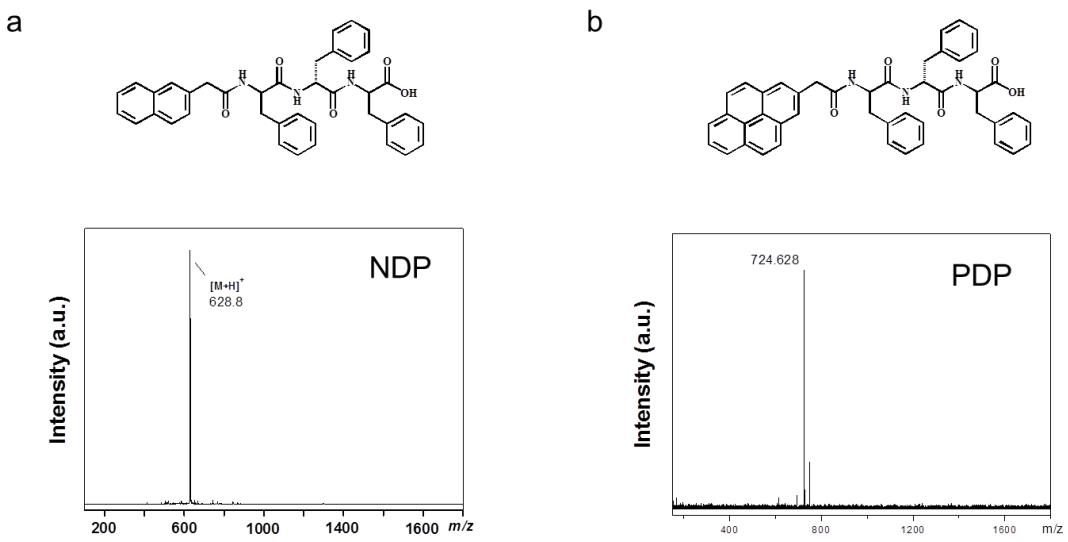

Supplementary Figure 3. MALDI-TOF-MS spectra of NDP and PDP. MALDI-TOF-MS spectra of the naphthalene-conjugated D-peptide, NDP (**a**), and the pyrene-conjugated D-peptide PDP (**b**).

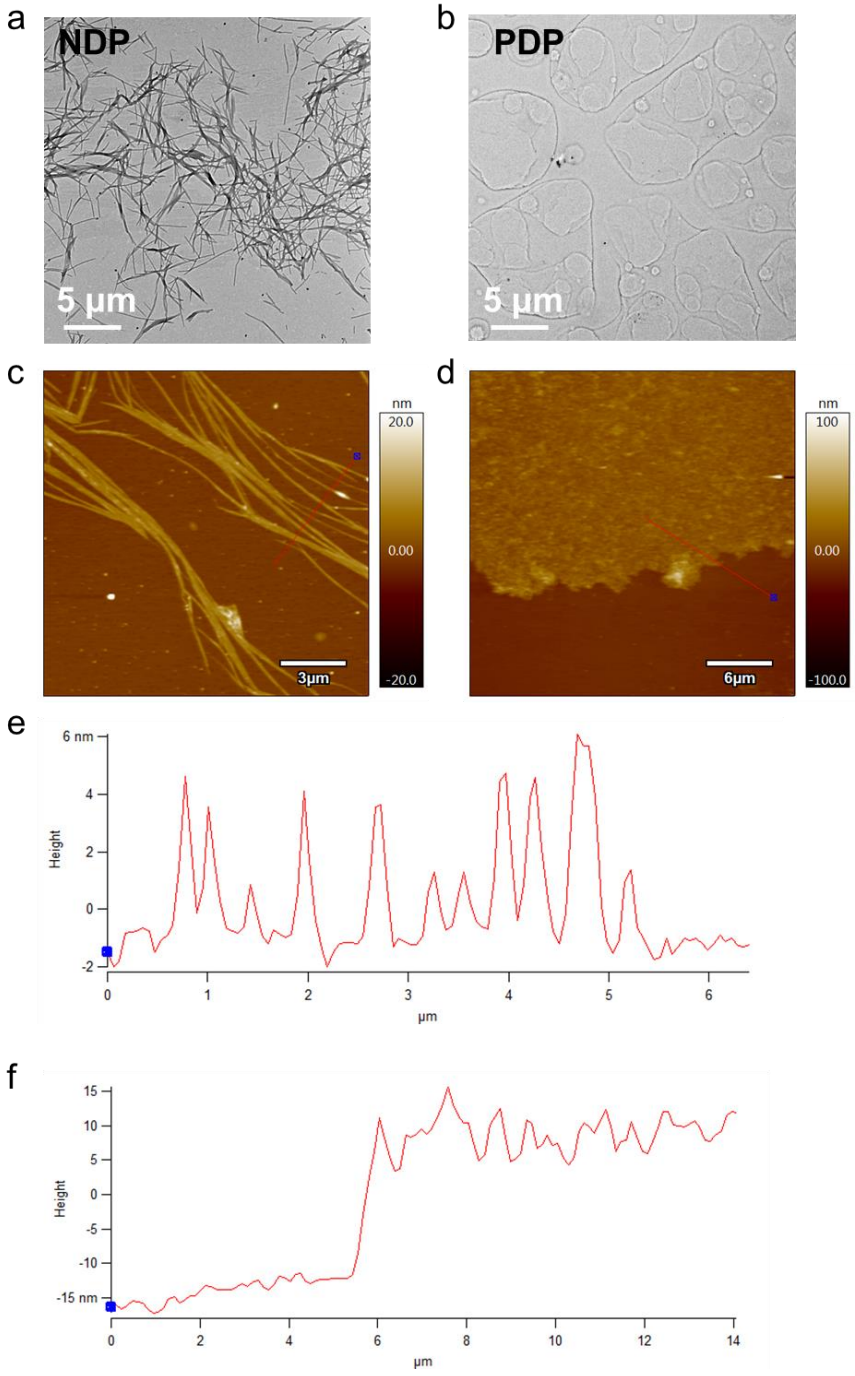

Supplementary Figure 4. Characterizations of the self-assembled NDP and PDP. (**a-b**) TEM and (**c-d**) AFM images of the self-assembled NDP and PDP, respectively. Experiments were performed for at least three times. (**e-f**), Height of the self-assembled nanostructures measured by AFM. Experiments were performed for at least three times. Scale bars in (**a-b**), 5 μm; Scale bar in (**c**) represents 3 μm; Scale bar in (**c**) represents 6 μm.

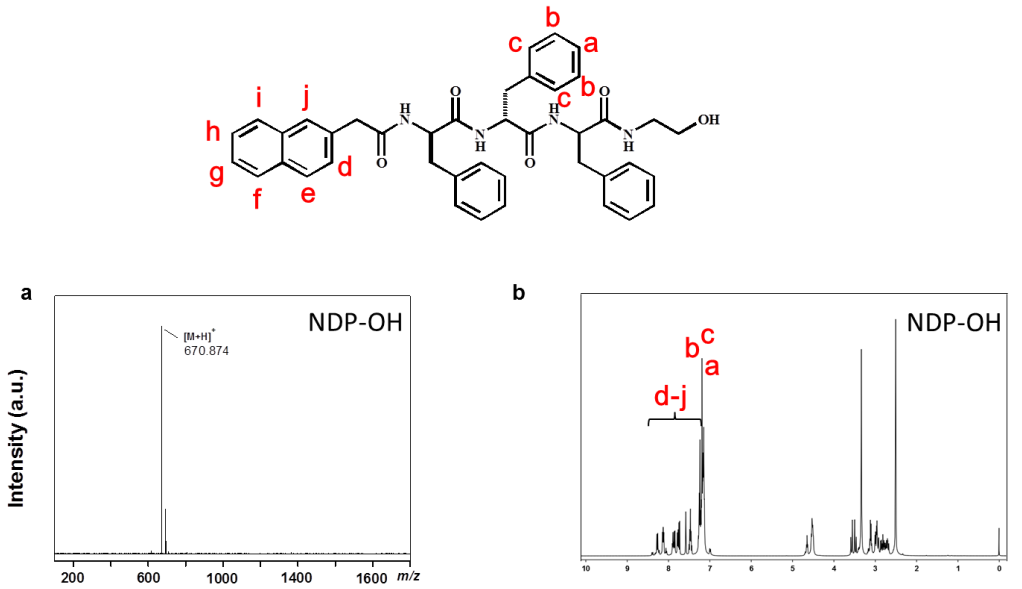

Supplementary Figure 5. MALDI-TOF-MS and ^{1}H-NMR spectrum of hydroxylated NDP. MALDI-TOF-MS (**a**) and ^{1}H-NMR spectrum (**b**) of hydroxylated NDP (NDP-OH).

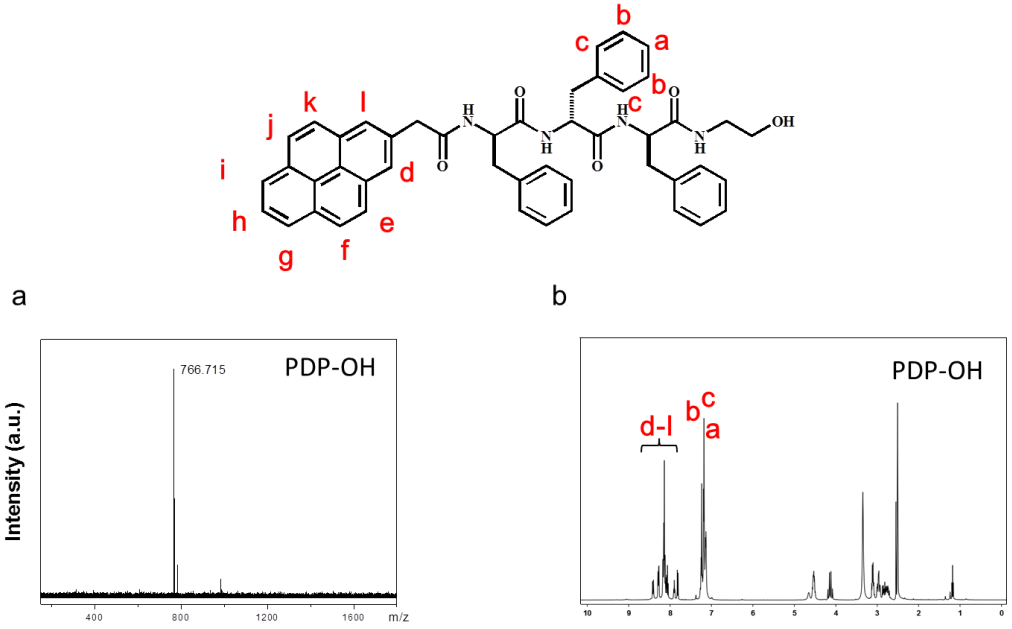

Supplementary Figure 6. MALDI-TOF-MS and ^{1}H-NMR spectrum of hydroxylated NDP. MALDI-TOF-MS (**a**) and ^{1}H-NMR spectrum (**b**) of hydroxylated PDP (PDP-OH).

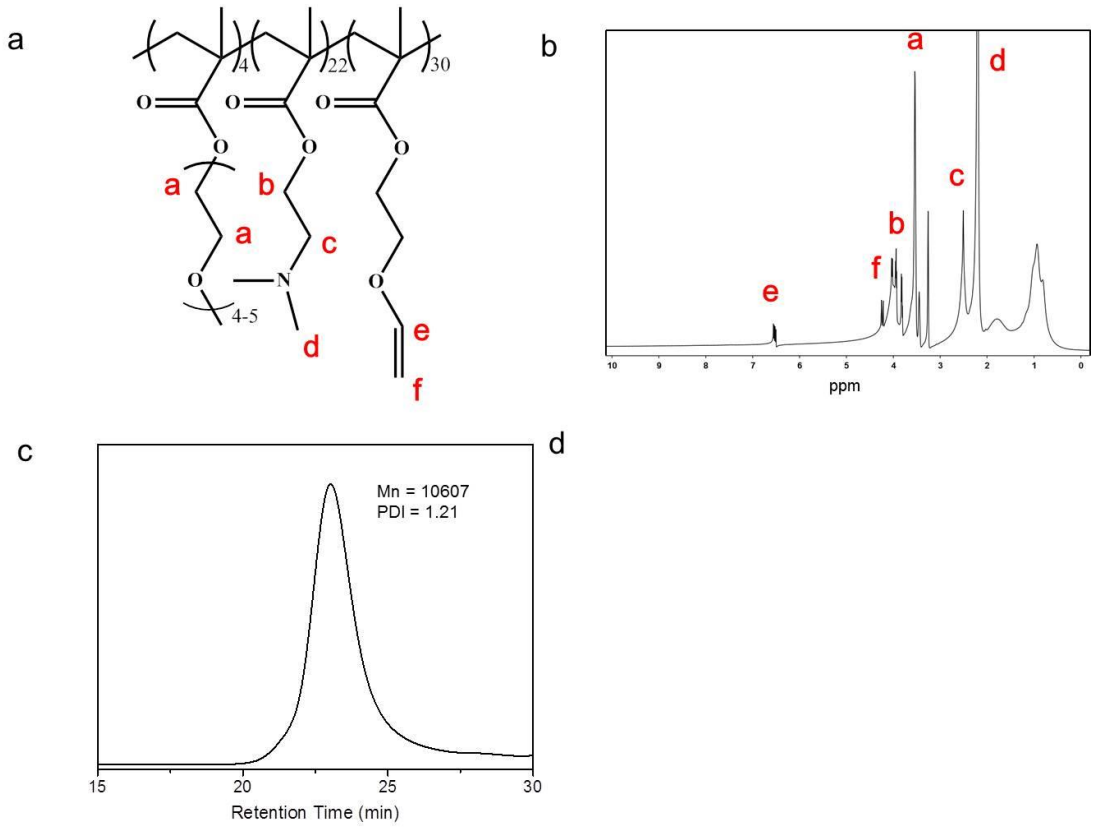

Supplementary Figure 7. Characterization of p(OEGMA$_4$-DMAEMA$_{22}$)-*b*-p(MAVE)$_{30}$. Structure (**a**), ^{1}H-NMR spectrum (**b**) and GPC trace (**c**) of p(OEGMA$_4$-DMAEMA$_{22}$)-*b*-p(MAVE)$_{30}$.

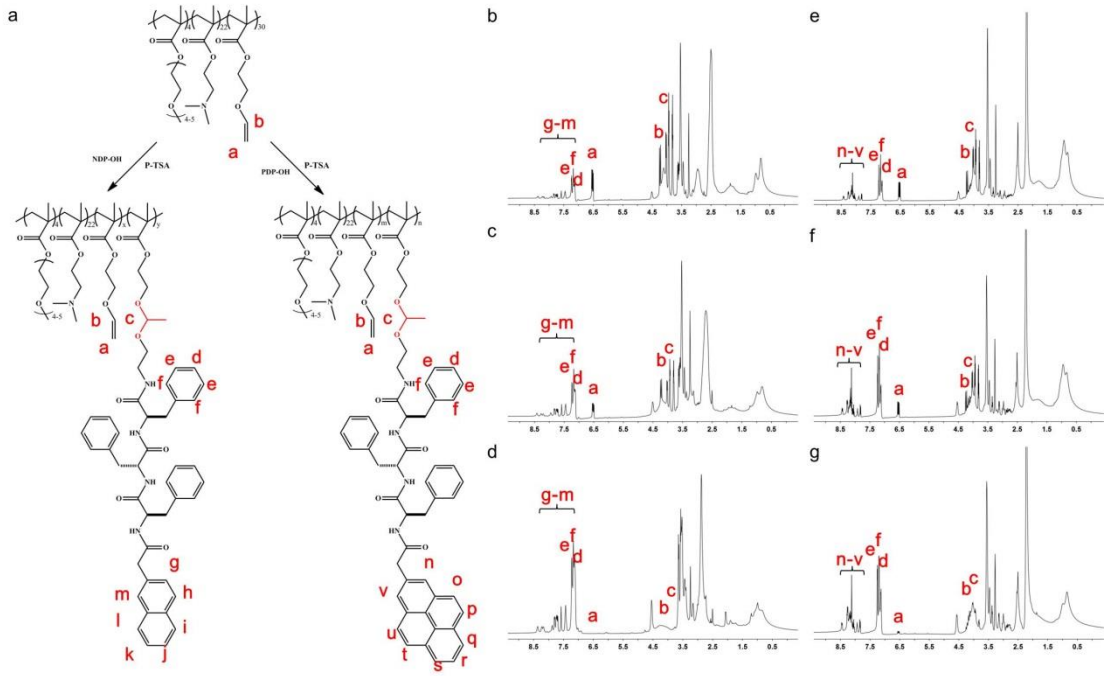

Supplementary Figure 8. ^{1}H-NMR spectra of the as-synthesized polymer-peptide conjugates. (**a**), Synthetic route for p(OEGMA$_4$-DMAEMA$_{22}$)-*b*-p((MAVE)$_x$-(MAVE-NDP)$_y$) and p(OEGMA$_4$-DMAEMA$_{22}$)-*b*-p((MAVE)$_m$-(MAVE-NDP)$_n$)., where x + y = 30, m + n = 30. (**b**), (**c**) and (**d**), ^{1}H-NMR spectra of p(OEGMA$_4$-DMAEMA$_{22}$)-*b*-p((MAVE)$_{25}$-(MAVE-NDP)$_5$), p(OEGMA$_4$-DMAEMA$_{22}$)-*b*-p((MAVE)$_{16}$-(MAVE-NDP)$_{14}$), and p(OEGMA$_4$-DMAEMA$_{22}$)-*b*-p((MAVE)$_8$-(MAVE-NDP)$_{22}$), respectively. (**e**), (**f**) and (**g**), ^{1}H-NMR spectra of p(OEGMA$_4$-DMAEMA$_{22}$)-*b*-p((MAVE)$_{25}$-(MAVE-PDP)$_5$), p(OEGMA$_4$-DMAEMA$_{22}$)-*b*-p((MAVE)$_{18}$-(MAVE-PDP)$_{12}$), and p(OEGMA$_4$-DMAEMA$_{22}$)-*b*-p((MAVE)$_9$-(MAVE-PDP)$_{21}$), respectively.

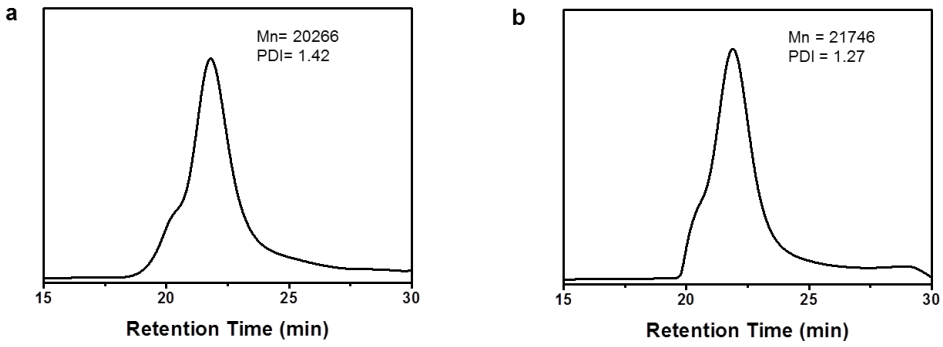

Supplementary Figure 9. GPC traces of the polymer-peptide conjugates. (**a**), p(OEGMA$_4$-DMAEMA$_{22}$)-*b*-p((MAVE)$_{16}$-(MAVE-NDP)$_{14}$), and (**b**), p(OEGMA$_4$-DMAEMA$_{22}$)-*b*-p((MAVE)$_{18}$-(MAVE-PDP)$_{12}$).

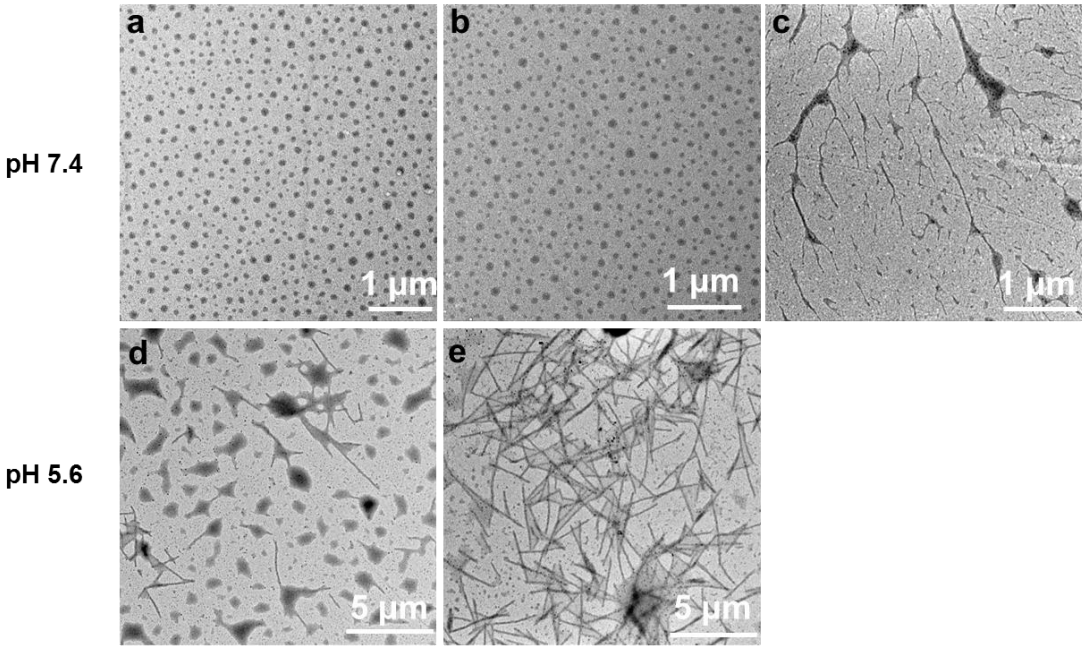

Supplementary Figure 10. The effects of peptides conjugation amount on the morphology and the pH-responsive re-assembly nature of the naontransformers. (**a**), (**b**) and (**c**) are TEM images of p(OEGMA$_4$-DMAEMA$_{22}$)-*b*-p((MAVE)$_x$-(MAVE-NDP)$_y$) with average NDP conjugation number of 5, 14 or 22. Scale bars: 1 μm. (**d**) and (**e**) are particles with average 5 or 14 NDP conjugation that incubated in acetate buffer (pH 5.6) for 10 min. Scale bar in (**d**) represents 1 μm; Experiments in (**a-e**) were performed for at least three times.

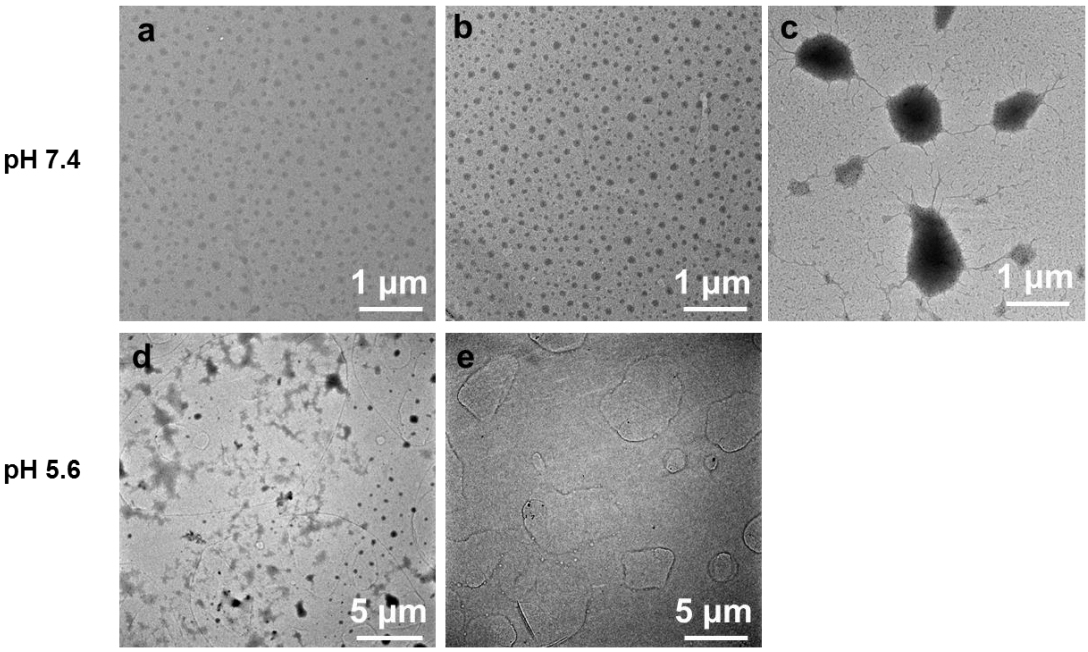

Supplementary Figure 11. The effects of the level of peptide conjugation on the morphology and the pH-responsive re-assembly of the nanotransformers. (**a**), (**b**) and (**c**) are TEM images of p(OEGMA$_4$-DMAEMA$_{22}$)-*b*-p((MAVE)$_m$-(MAVE-PDP)$_n$) with an average PDP conjugation number of 5, 12 or 21, respectively. Scale bars: 1 μm. (**d**) and (**e**) are nanoparticles with an average PDP conjugation number of 5 or 12, respectively, after incubation in acetate buffer (pH 5.6) for 10 min. Scale bars: 5 μm. p(OEGMA$_4$-DMAEMA$_{22}$)-*b*-p((MAVE)$_9$-(MAVE-PDP)$_{21}$) with 21 PDP conjugations aggregates in PBS and cannot form nanoparticle. Experiments in (**a-e**) were performed for at least three times.

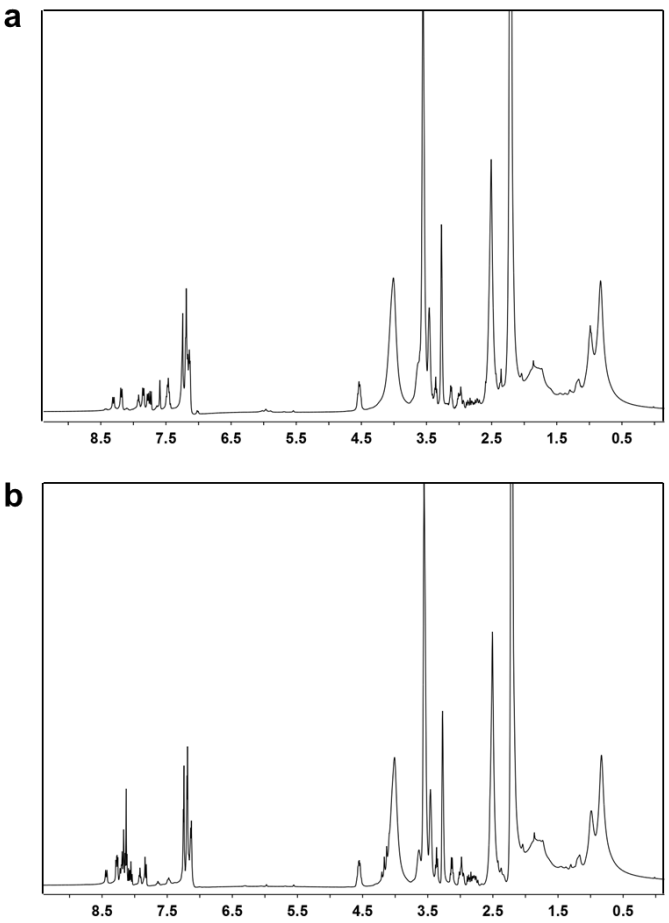

Supplementary Figure 12. ^{1}H-NMR spectra of polymer-peptide conjugates with non-pH-sensitive ether bonds. (**a**), and (**b**), ^{1}H-NMR spectra of p(DMAEMA$_{22}$-OEGMA$_{4}$)-*b*-p((MA)$_{15}$-(MA-NDP)$_{15}$), (NR1) and p(DMAEMA$_{22}$-OEGMA$_{4}$)-*b*-p((MA)$_{16}$-(MA-PDP)$_{14}$), (NR2), respectively.

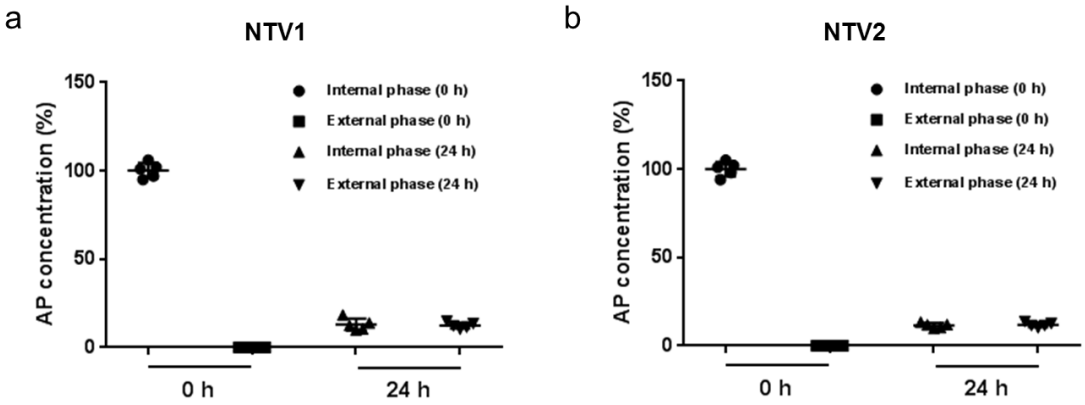

Supplementary Figure 13. Dialysis experiment determines the interaction between peptide and polymer. NTV1 or NTV2 were mixed with AP in 1 mL PBS and then dialyzed against 10 mL PBS (pH 7.4) for 24 h. After that, the AP concentration in the dialysis bag (internal phase) and the external phase were determined using HPLC. Data were shown as means ± s.d. (n = 5) from five independent experiments.

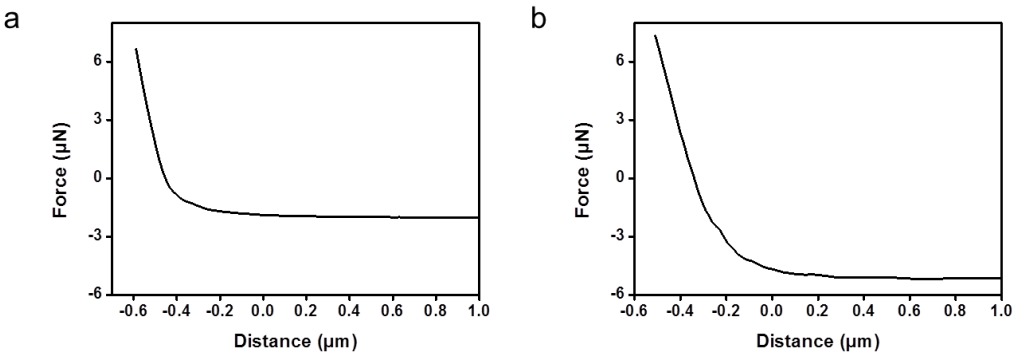

Supplementary Figure 14. Representative force vs distance curves for the re-assembled NTV1 and NTV2 in a mimic endosomal environment. NTV1 (**a**) or NTV2 (**b**) was incubated in acetate buffer (pH = 5.6) for 10 min and then the Young's modulus of the re-assembled nanostructures in the acetate buffer was measured using an atomic force microscope. Experiments were performed for at least three times.

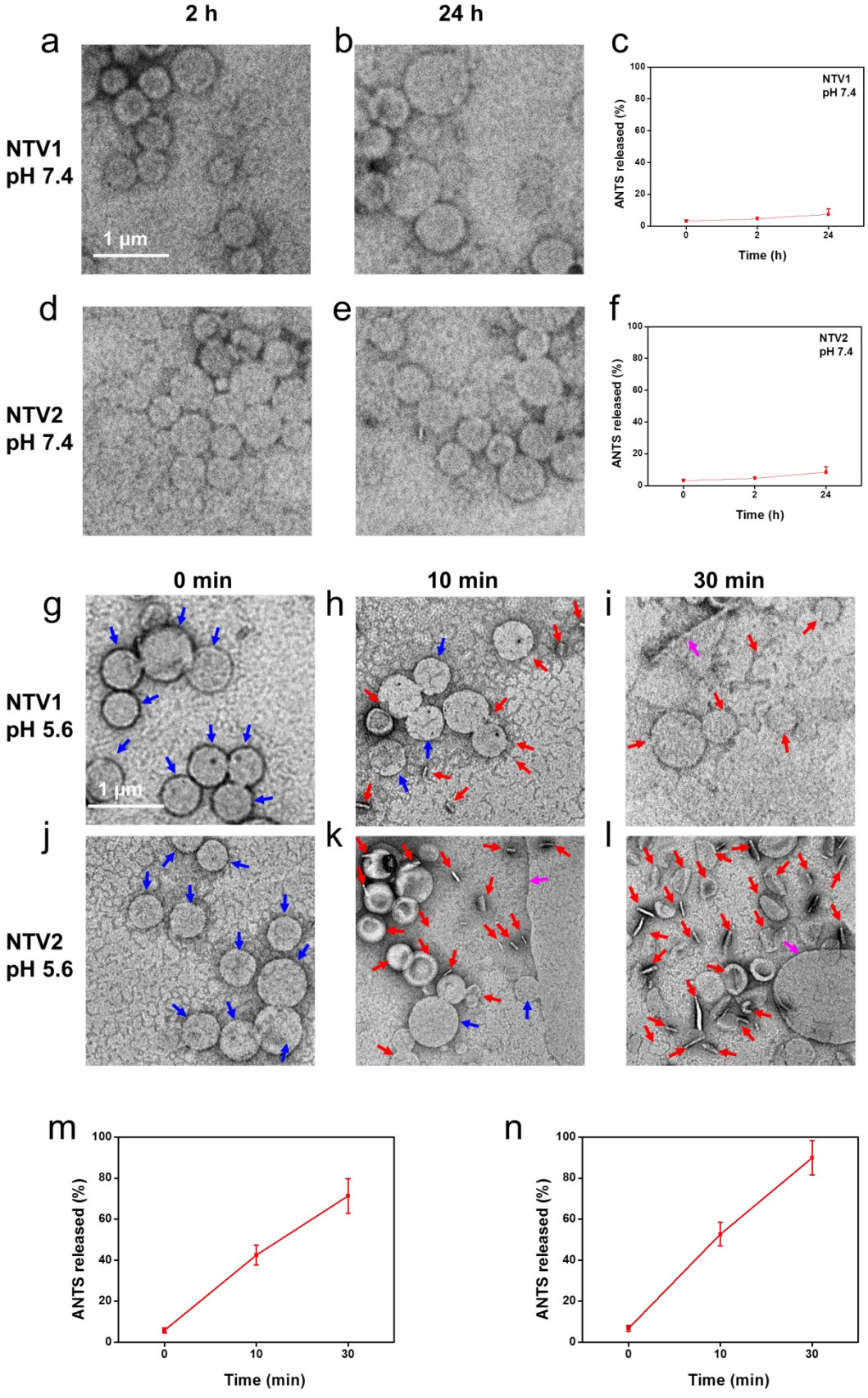

244

245 **Supplementary Figure 15. NTV1 and NTV2 induce artificial endosomes disruption at**

246 **pH 5.6.** In order to demonstrate the stability of NTV1 and NTV2 in pH 7.4 buffer, we

incubated NTV1-loaded AEs and NTV2-loaded AEs in a pH 7.4 buffer and the morphology of the nanoparticle-loaded AEs were observed at different time points using TEM. (**a**) and (**b**), TEM images of NTV1-loaded AEs incubated in pH 7.4 buffer for 2 h and 24 h, respectively. Experiments were performed for at least three times. And (**c**) shows a dye-release profile from the NTV1-loaded AEs at indicated time. Data were shown as mean ± s.d. (n = 3) from three independent experiments. (**d**) and (**e**), TEM images of NTV2-loaded AEs incubated in pH 7.4 buffer for 2 h and 24 h, respectively. Experiments were performed for at least three times. And (**f**) shows a dye-release profile from the NTV1-loaded AEs at indicated time. Data were shown as mean ± s.d. (n = 3) from three independent experiments. (**g-i**), TEM images of NTV1-loaded AEs incubated in pH 5.6 buffer for 0 min (**g**), 10 min (**h**) and 30 min (**i**). Experiments were performed for at least three times. (**j-l**), TEM images of NTV2-loaded AEs incubated in pH 5.6 buffer for 0 min (**j**), 10 min (**k**) and 30 min (**l**). Experiments were performed for at least three times. And dye release from NTV1-or NTV2-loaded AEs at different time points were also investigated (**m-n**). Data were shown as mean ± s.d. (n = 3) from three independent experiments. TEM images in (**a-b**, **d-e** and **g-l**) were obtained under a HT7700 bio-TEM, samples were negatively stained before observation. Dye release experiments were performed as detailed described in the Supplementary information. Blue arrows indicate the intact AEs; red arrows indicate the damaged AEs or small pieces of the AEs; Pink arrows indicate the re-assembled nanostructures. Pink arrow in (**k**) indicate the edge of a very large re-assembled nanosheet; Pink arrow in (**l**) indicate a small re-assembled nanosheet; Pink arrow in (**l**) indicate a small re-assembled nanosheet; Though NTV1 also induced the damage of AEs, but most of the reassembled structures was trapped in the AEs, only very few nanofiber structures can be observed under TEM (pink arrow in (**i**)). Scale bars: 1 μm.

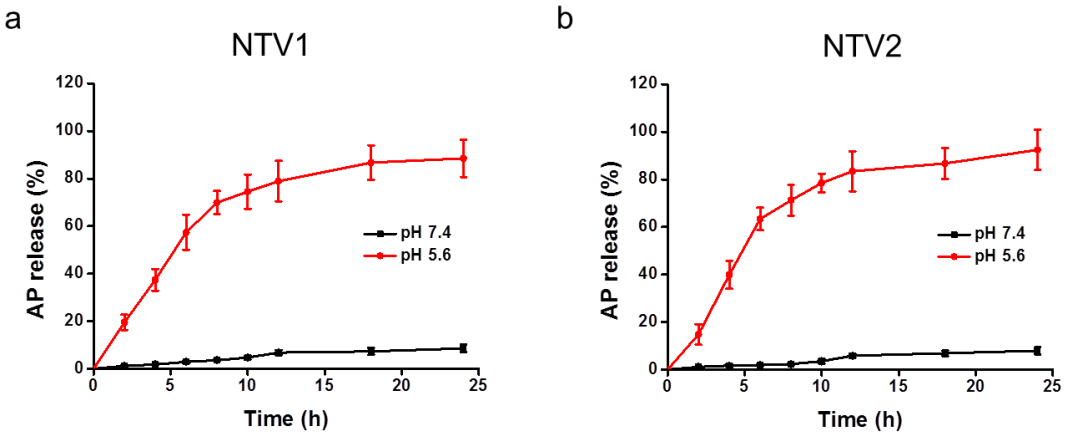

Supplementary Figure 16. AP release from vaccines under different pH values. AP ($OVA_{241-270}$) releases from NTV1 (**a**) or NTV2 (**b**) under pH 7.4 or pH 5.6 were analyzed. Experiments were performed four times, data were shown as mean ± s.d. (n = 4) from four independent experiments.

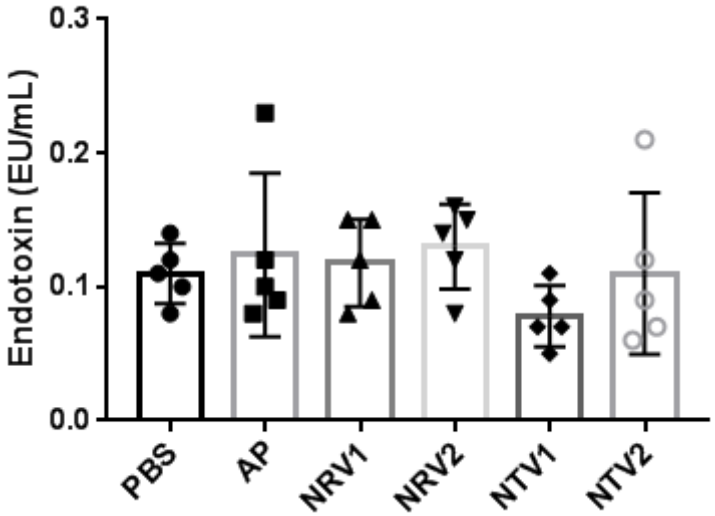

Supplementary Figure 17. Endotoxin level of the formulations. Endotoxin levels of the formulations were detected via chromogenic LAL endotoxin assay kit. Data were shown as mean ± s.d. (n = 4) from four independent experiments.

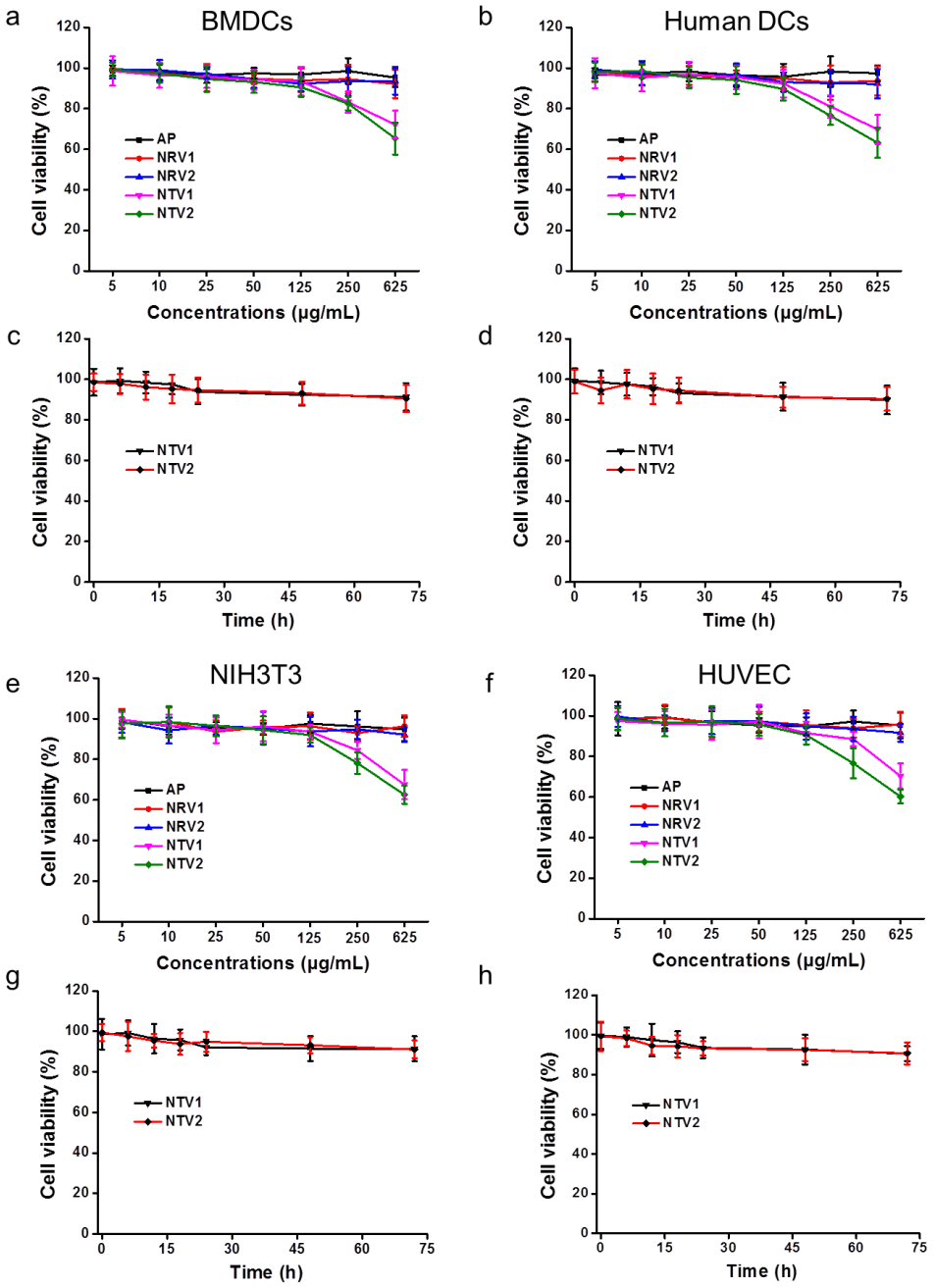

Supplementary Figure 18. Cytotoxicity of the nanovaccines in BMDCs and human DCs. BMDCs, human DCs, NIH3T3 cells, HUVEC cells were incubated with different concentrations of AP, NRV1, NRV2, NTV1 or NTV2 for 24 h and the cell viability were determined using cck-8 (**a-b, e-f**). (**c-d, g-h**), the cell viability of NTV1 or NTV2 treated cells at different time points (0, 6, 12, 18, 24, 48 and 72h), determined by cck-8 kit. Data in (**a-h**) were shown as means ± s.d. (n = 3) from three independent experiments.

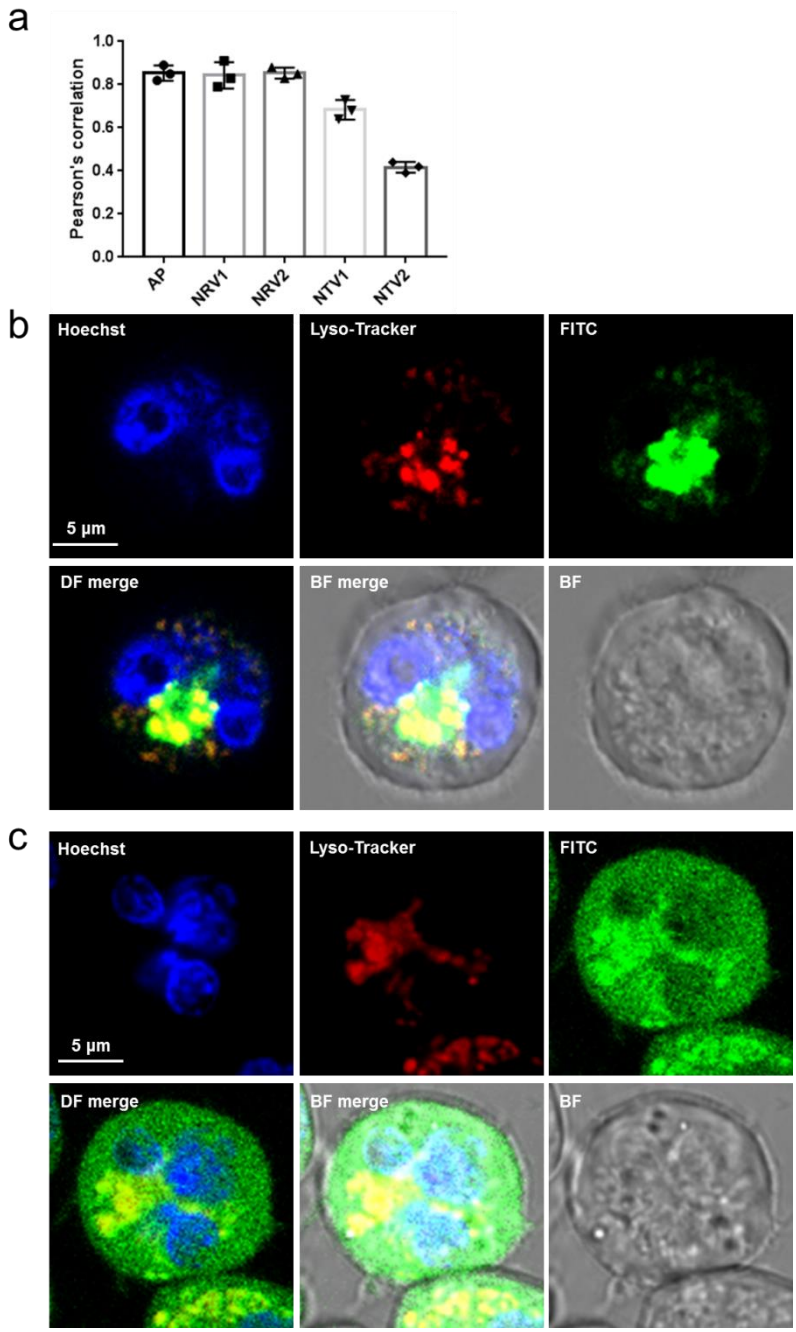

Supplementary Figure 19. Intracellular distribution of AP-FITC. (**a**), Quantification of fluorescence co-localization between AP-FITC and LysoTracker after DC2.4 cells were incubated with free AP-FITC, NRV1, NRV2, NTV1 or NTV2 for 24 h. 3 images (~15 cells) were analyzed in each group and data were shown as mean ± s.d. (n = 3) from three independent experiments. Pearson's correlations were calculated using Image-pro Plus 6.0 software. (**b**) and (**c)** are higher magnification images of the distribution of AP-FITC in free AP-FITC treated cells (**b**) or AP-FITC-loaded NTV2 treated DC2.4 cells (**c**), respectively. Scale bar: 5 μm. Experiments in (**b-c**) were performed for at least three times.

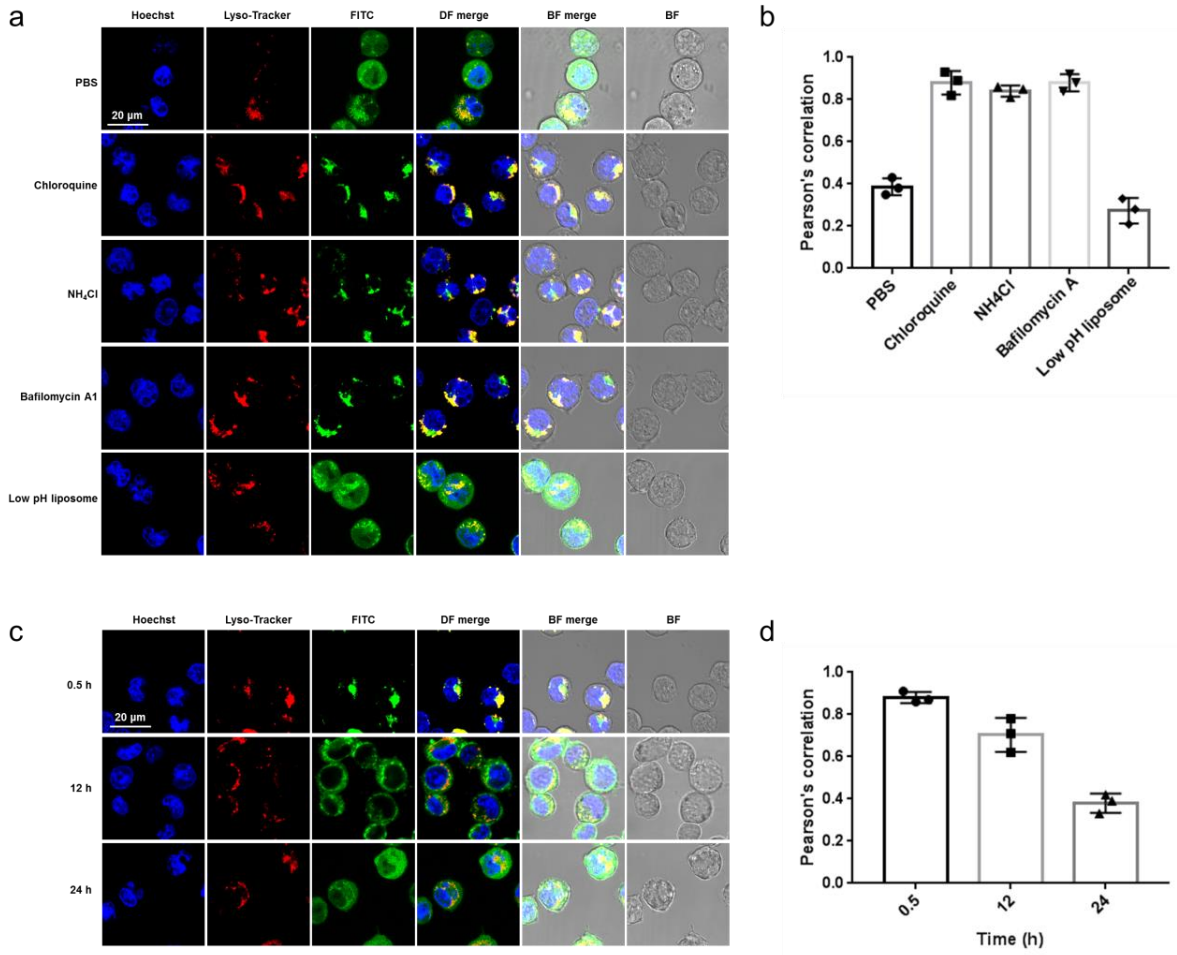

305

306 **Supplementary Figure 20. Intracellular distribution of NTV2.** (**a**), Distributions of the
307 antigenic peptide ($OVA_{241-270}$-FITC, delivered by NTV2) in PBS, chloroquine, NH_4Cl,
308 bafilomycin A1 or acidic liposome pre-treated DC2.4 cells. Chloroquine, NH_4Cl and
309 bafilomycin A1 can increase the pH value in endosome and acidic liposome was reported
310 to increase the endosomal pH in cells. Experiments were performed for at least three
311 times. Scale bar: 20 μm. (**b**), Quantification of fluorescence co-localization between
312 AP-FITC and Lyso-Tracker. 3 images (~15 cells) were analyzed in each group and data
313 were shown as mean ± s.d. (n = 3) from three independent experiments. Pearson's
314 correlations were calculated using Image-pro Plus 6.0 software. (**c**), Intracellular
315 distribution of $OVA_{241-270}$-FITC at 0.5 h, 12 h and 24h after NTV2 incubation. Experiments
316 were performed for at least three times. Blue, nucleus; red, late endosomes stained with
317 Lyso-Tracker Deep Red; green, $OVA_{241-270}$-FITC. Scale bar: 20 μm. (**d**), Quantification of
318 fluorescence co-localization between AP-FITC and Lyso-Tracker. 3 images (~15 cells)
319 were analyzed in each group and data were shown as mean ± s.d. (n = 3) from three
320 independent experiments. Pearson's correlations were calculated using Image-pro Plus
321 6.0 software.

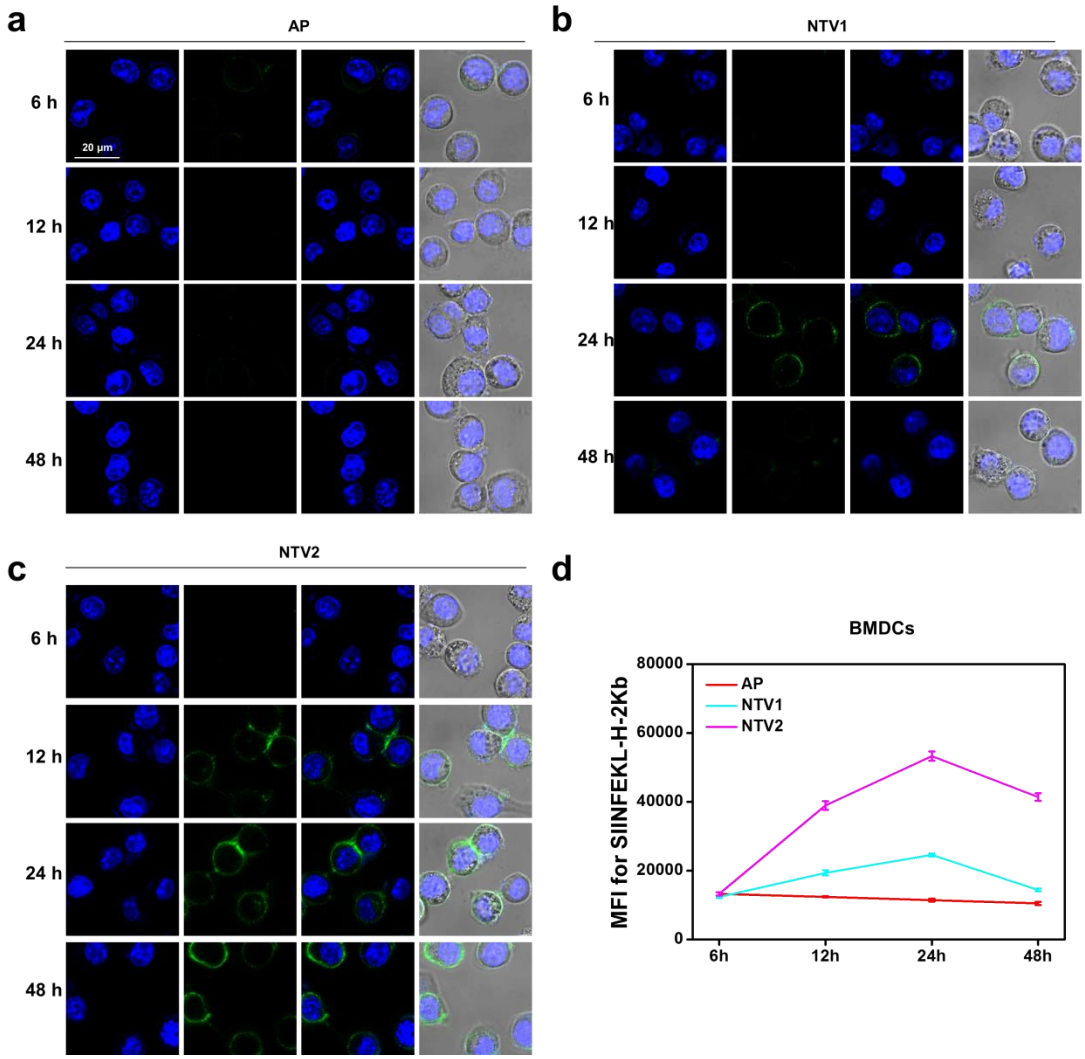

Supplementary Figure 21. Surface-presentation of AP in DC2.4 and BMDCs. BMDCs were incubated with free AP ($OVA_{241-270}$), NTV1 or NTV2 with an equivalent AP concentration of 5 μg/mL for 6, 12, 24 or 48 h. Then the cells were stained with SIINFEKL-H-$2K^b$-specific monoclonal antibody and observed under CLSM (**a-c**) and flow cytometry (**d**). Data from three independent experiment were shown as means ± s.d. (n = 3) from three independent experiments. Scale bar in (**a**) represents 20 μm.

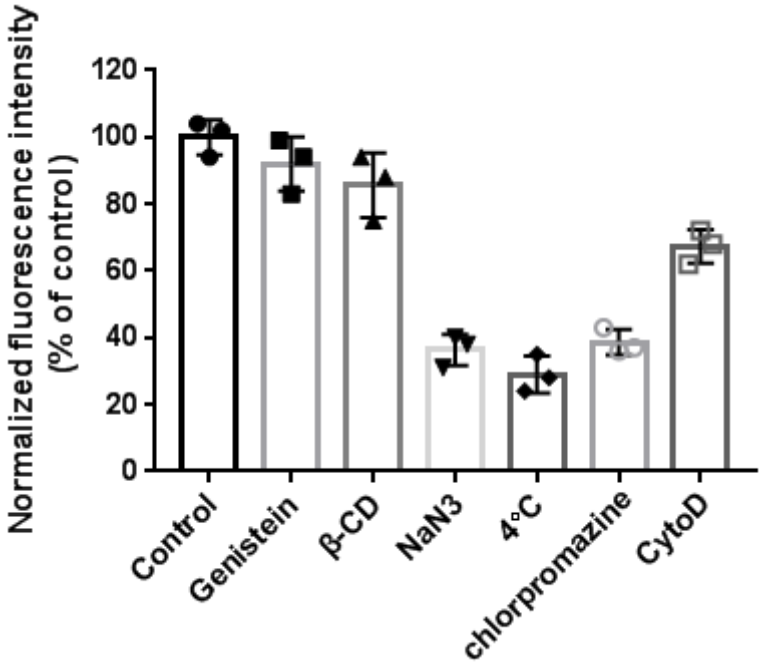

Supplementary Figure 22. Investigation of the cellular uptake mechanism of NTV2 using endocytosis inhibitors. BMDCs were incubated with various inhibitors as follows: genistein (200 μM), methyl-β-cyclodextrin (β-CD, 5 mM), 0.1% NaN_3/50 mM 2-deoxyglucose, low temperature (4 °C), chlorpromazine (10 μg/mL) or cytochalasin D (CytoD) (5 μg/mL) for 30 min. Cells were then cultured with $OVA_{241-270}$-FITC loaded NTV2 (at nanoparticle concentration of 125 μg/mL) for 30 min. Percent internalization was normalized to NTV2 uptake in the inhibitor-free group. Data from three independent experiments were shown. Data were shown as means ± s.d. (n = 3) from three independent experiment.

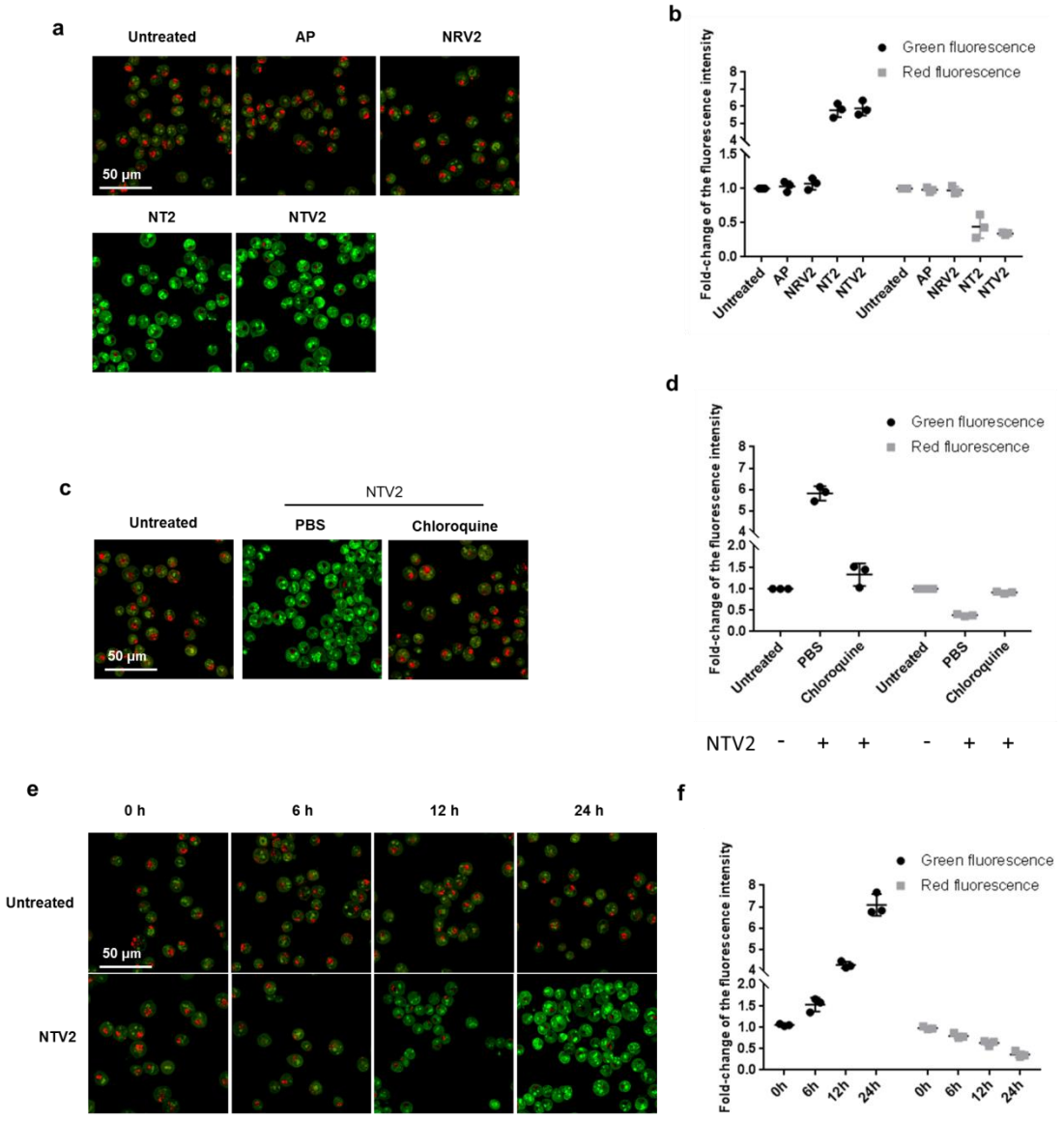

Supplementary Figure 23. The effects of different formulations on endosome membrane integrity investigated by acridine orange staining assay. (**a**), DC2.4 cells were treated with AP alone, NR2, NT2, or NTV2 (at nanoparticle dose of 125 μg/mL) for 24 h. The cells were rinsed with PBS, then incubated with 2.5 μg/mL AO for 15 min and finally observed under CLSM. Untreated DC2.4 cells were used as a negative control. Scale bar: 50 μm. (**b**), Fold-change of the green and red fluorescence intensity after various formulations treatment (compared to the fluorescence in untreated cells). (**c**), cells were pre-treated with chloroquine (increase the pH in endosome) and incubated with NTV2 for 24 h, then AO staining was performed and the fluorescence of AO were observed under CLSM. Scale bar: 50 μm. (**d**), Fold-change of the green and red fluorescence intensity in (**c**), compared to the untreated cells. (**e**), DCs were treated with NTV2 for 6h, 12h or 24h, and then the cells were stained with AO and observed under CLSM. Scale bar: 50 μm. And (**f**), quantification of (**e**). All the experiments were performed at least three times, in (**b**), (**d**) and (**f**), data were shown as means ± s.d (n = 3) from three independent experiments.

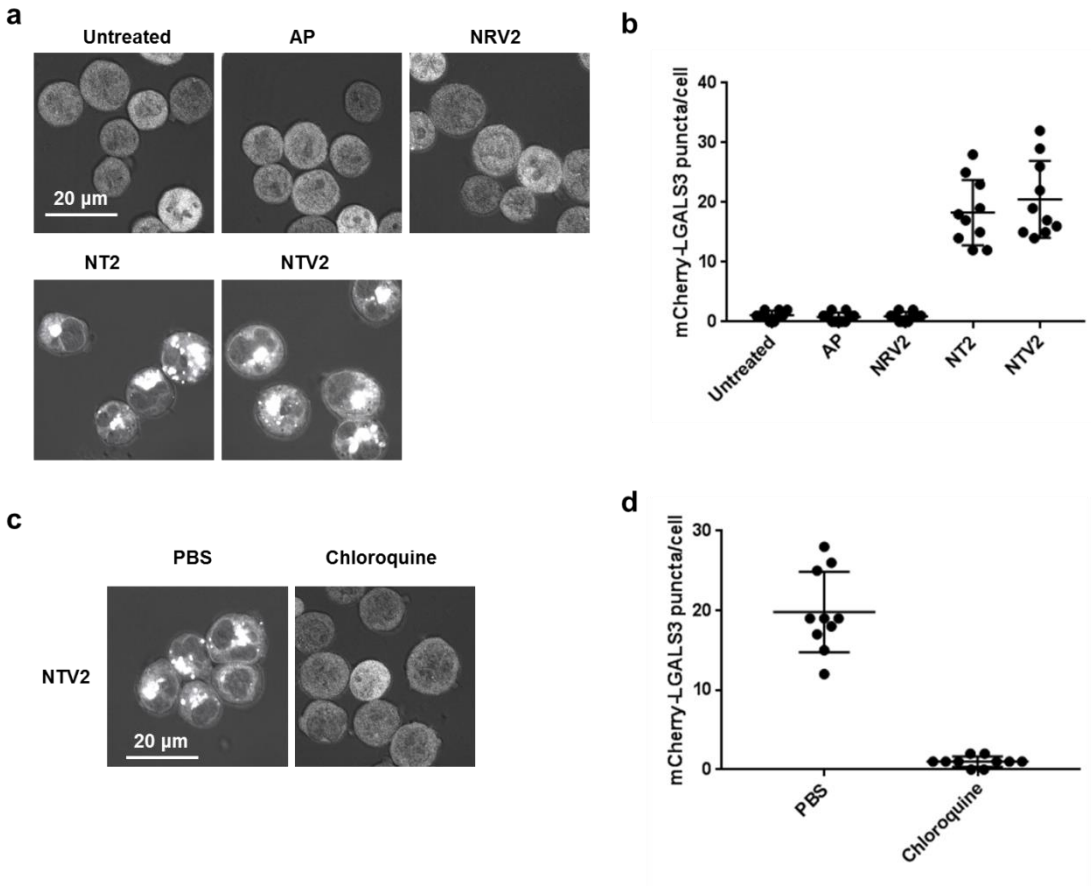

Supplementary Figure 24. Endosomal membrane permeability evaluated by a galectin puncta assay. (**a**), DC2.4-mCherry-LGALS3 cells were treated with free AP ($OVA_{241-270}$), NRV2, NT2 or NTV2 (at nanoparticle dose of 125 μg/mL) for 24 h and the cells were observed under CLSM. The formation of mCherry-LGALS3 puncta indicates endosomal membrane damage. Scale bar: 20 μm. (**b**), quantification of the average number of mCherry-LGALS3 puncta in each cell (at least 10 cells were analyzed in each group). (**c-d**), Chloroquine pre-treatment reversed the endosomal membrane-disruption capacity of NTV2. Experiments were in performed at least three times, (**b**) and (**d**), data were shown as means ± s.d. (n = 10) from independent samples. Scale bar in (**c**) represents 20 μm.

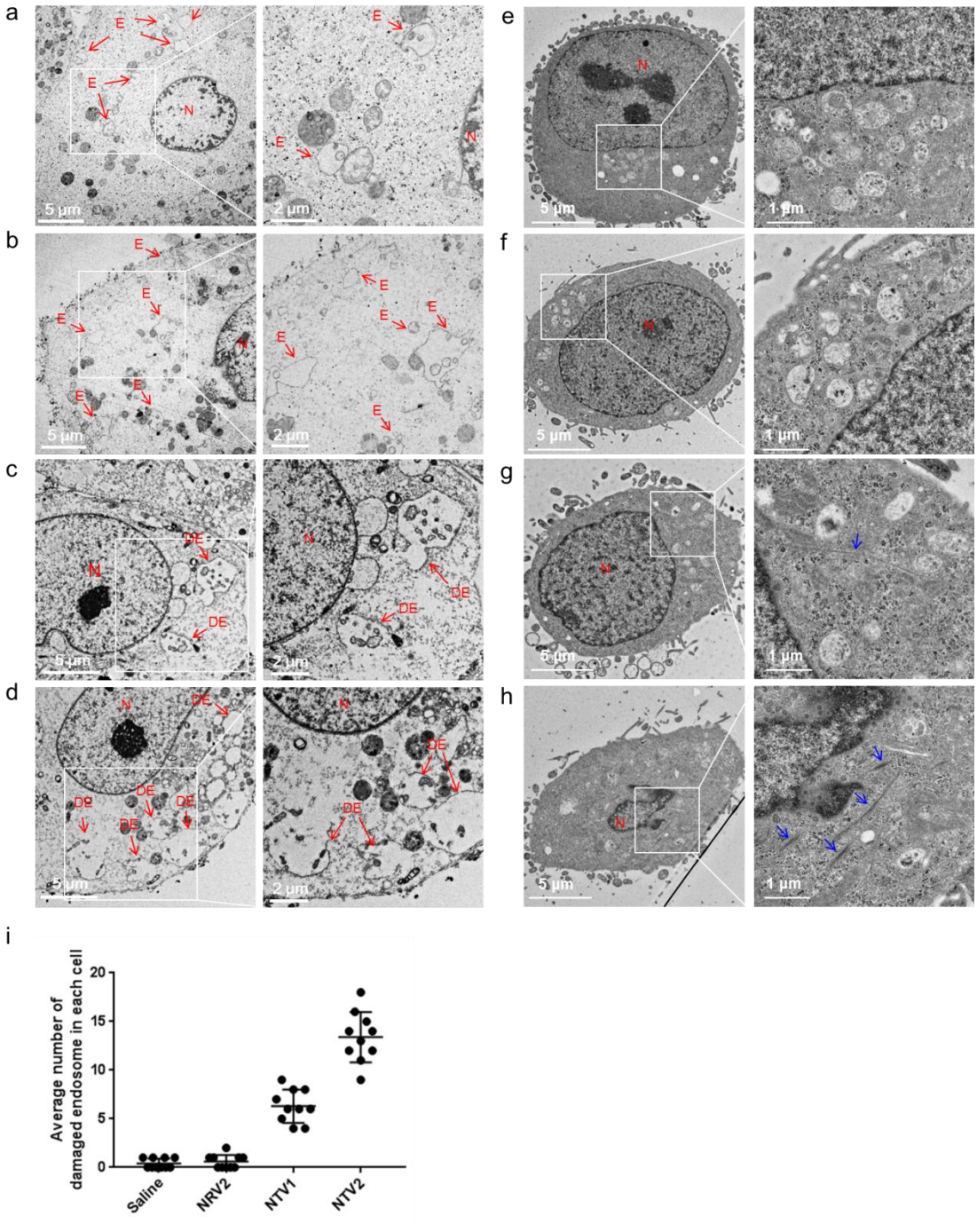

Supplementary Figure 25. NTV-induced endosome disruption observed under Bio-TEM. DC2.4 cells were incubated with NTV1 or NTV2 for 24 h (at a nanoparticle dose of 125 μg/mL)) and then the cells were fixed, sectioned and observed under Bio-TEM. Images of DC2.4 cells treated with saline (**a**), NRV2 (**b**), NTV1 (**c**) and NTV2 (**d**). N, nucleus; E, endosome; DE, disrupted endosome. Experiments were performed for at least three times. In order to see the re-assembled nanstructures more clearly, we extended the uranyl acetate staining time in (**e-h**). (**e-h**), image of saline (**e**), NRV2 (**f**), NTV1 (**g**), and

NTV2 (**h**)-treated DC 2.4 cells (N, nucleus; red arrows, re-assembled nanostructures), $OVA_{257-264}$ was used as a model AP in this experiment. Experiments were performed for at least three times. But the extended staining time induced a darker background and less detailed information of the cytoplasm. The endo/lysosome in the PBS treated group showed normal structure and with numbers of about 15 endo/lysosomes can be observed in each cell. However, less endo/lysosome in the cytoplasm of NTV1 and NTV2 treated cells can be observed, which is because the damaged endo/lysosome structures are open to cytoplasm and the protein and lipid drops-rich cytoplasm can easily spread to the damaged endo/lysosome. And longer staining time led to the proteins and lipid drops also been stained. Thus, the broken endo/lysosome cannot be observed very clearly in these pictures. However, we can see some fiber-like structures exist in the cell cytoplasm in NTV1 and NTV2 treated cells. And the NTV2 nanoparticle treated cells showed highest number of fiber-like structures. The reason that we only see the fiber but not see the sheets in (**h**) is because the cell section is only 70 nm thickness and the section direction was not on the same layer with the nanosheets. Blue arrows, re-assembled nanostructures. (**i**), Average number of the damaged endosomes in each cell (10 cells were analyzed in each group). Experiments were performed at least three times.

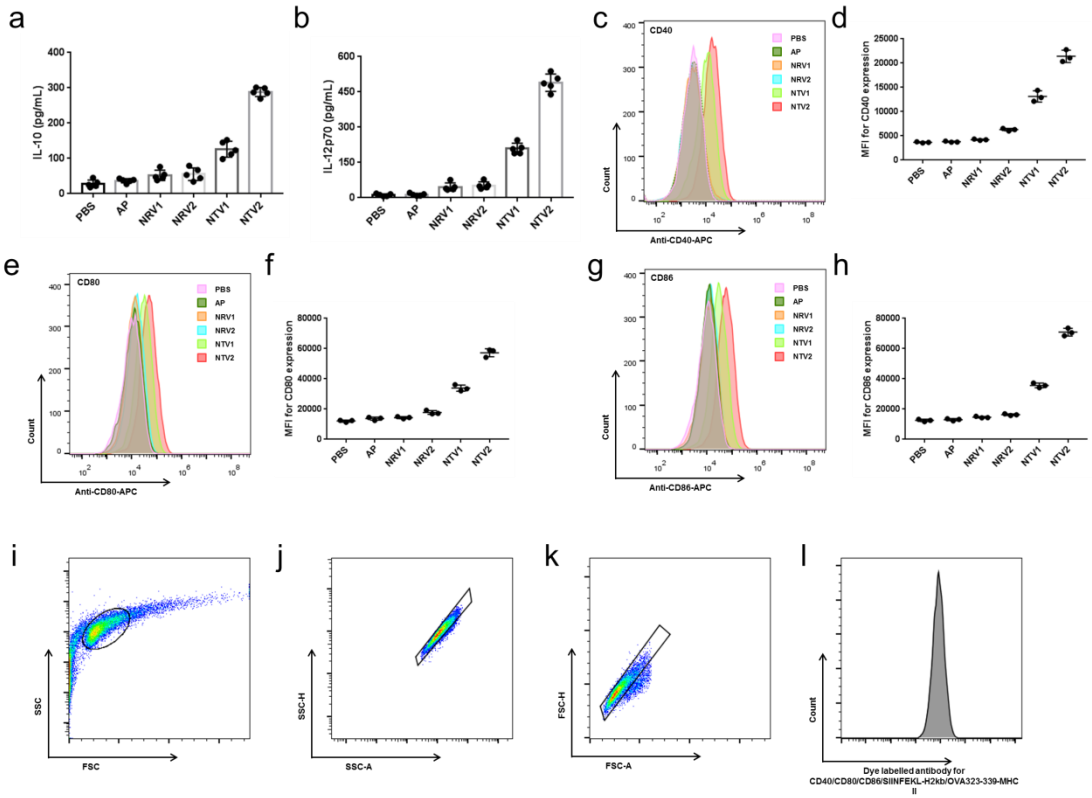

Supplementary Figure 26. NTV induce dendritic cell maturation *in vitro*. (**a-b**), IL-10 (**a**) and IL-12p70 (**b**) concentrations in the medium after BMDCs were treated with various $OVA_{241-270}$-loaded formulations (at an equivalent AP dose of 5 μg/mL) for 24 h. Experiments were performed five times, data were shown as mean ± s.d. (n = 5) from five independent experiments. (**c-h**) BMDCs were treated with various $OVA_{241-270}$-loaded formulations for 24 h and the DC maturing markers CD40 (**c-d**), CD80 (**e-f**) and CD86 (**g-h**) were determined by flow cytometer. Experiments were performed three times, data were shown as means ± s.d. (n = 3) from three independent experiments. (**i-l**), gating strategy for CD40, CD80, CD86 (**Supplementary Figure 26c-h**), SIINFEKL-H2Kb (**Supplementary Figure 21d**) or $OVA_{323-339}$-I-Ad complex (**Supplementary Figure 28a-b**).

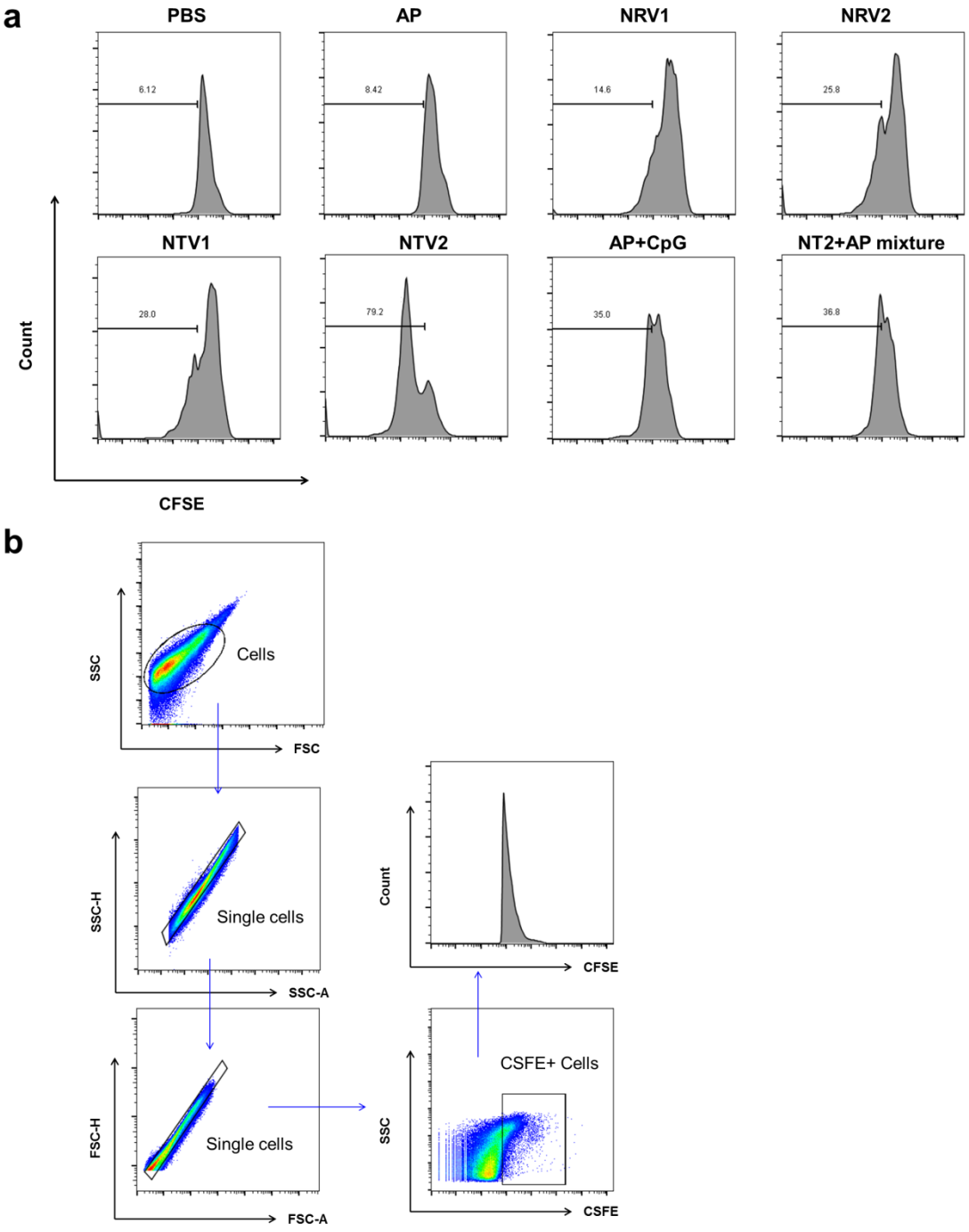

Supplementary Figure 27. OT-I cell proliferation assay. Mice were vaccinated with various $OVA_{241-270}$-loaded vaccine formulations for three times (every 7 days, at equivalent peptide dose of 5 μg/mice) and after 24h of the last vaccination, CFSE-labeled OT-I cells were i.v. injected to the vaccinated mice. After another 3 days, the mice were killed and the splenocyte were analyzed by flow (**a**). (**b**), gating strategy for the fluorescence (CSFE) dilution experiments in **Supplementary Figure 27** and **Supplementary Figure 28c**. All the experiments were performed at least three times.

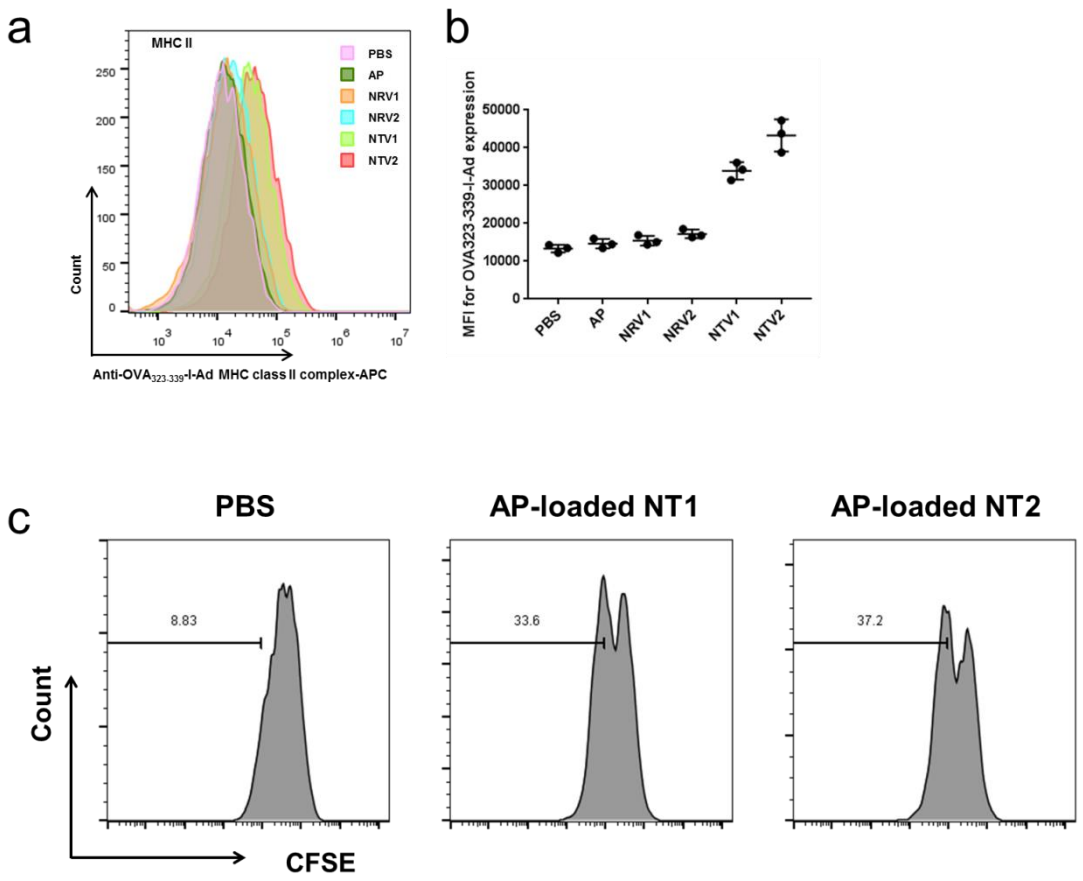

Supplementary Figure 28. Nanotransfmers for MHC II long peptide delivery. (**a-b**), BMDCs were treated with $OVA_{317-347}$-loaded formulations (at equivalent peptide dose of 5 μg/mice) for 24 h and $OVA_{323-339}$-I-Ad complex (epitope-MHC II) expression level on the surface of DCs were determined using flow cytometer. Experiments were performed three times, data in (**b**) were shown as mean ± s.d. (n = 3) from three independent experiments. (**c**) Mice were vaccinated with $OVA_{317-347}$-loaded NT2 for three times (every 7 days) and after 24h of the last vaccination, CFSE-labeled OT-II cells were i.v. injected to the vaccinated mice. After 3 days, the mice were killed and the splenocyte was analyzed by flow. Experiments were performed at least three times.

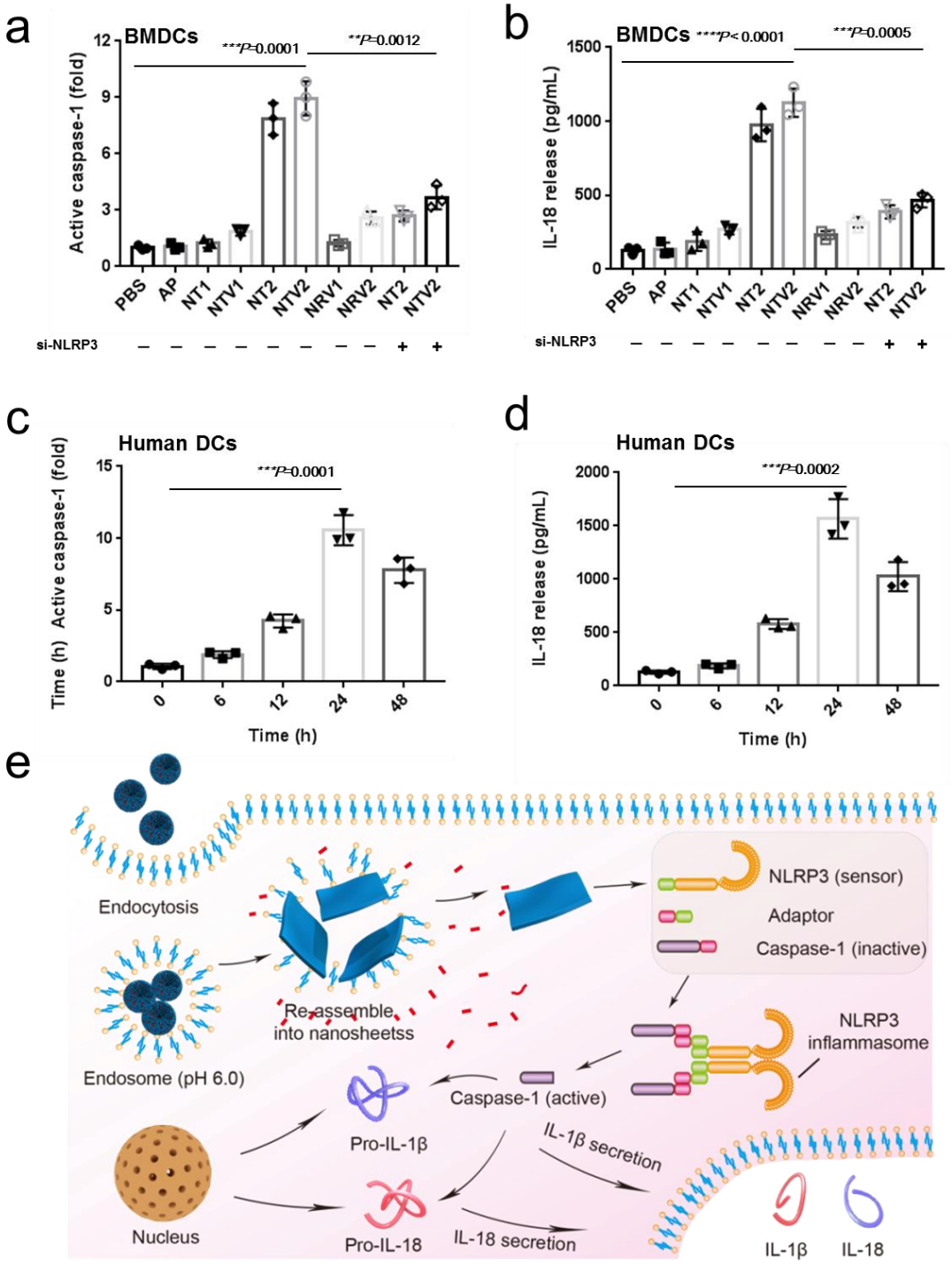

Supplementary Figure 29. NTV2 enhance the maturation of BMDCs by activating the NLRP3 inflammasome pathway. (**a**) and (**b**), Caspase-1 cleavag and IL-18 release from BMDCs after treatment with different formulations (at an equivalent AP dose of 5 μg/mL) were detected using a colorimetric caspase-1 activity detection kit or an ELISA kit for IL-18. Pre-treating cells with siRNA for NLRP3 was used as control. Experiments were performed for at least three times, data were shown as means ± s.d. (n = 3) form three independent experiments, by two-tailed unpaired Student's t-test, ****P* = 0.0001 for PBS versus NTV2 comparison in (**a**), ***P* = 0.0012 for NTV2 versus NTV2+siRNA comparison

in (**a**), ****P < 0.0001 for PBS versus NTV2 comparison in (**b**), ***P = 0.0005 for NTV2 versus NTV2+siRNA comparison in (**b**) (**c-d**), Dose-dependent caspase-1 cleavage and IL-18 release from human DCs. Data are shown as means ± s.d. (n = 3) form three independent experiments, by two-tailed unpaired Student's *t*-test, ***P = 0.0001 for 0 h versus 24 h comparison in (**c**), ***P = 0.0002 for 0 h versus 24 h in (**d**). (**e**), Proposed mechanism by which NTV2 activates the NOD-like receptor to promote the maturation of BMDCs.

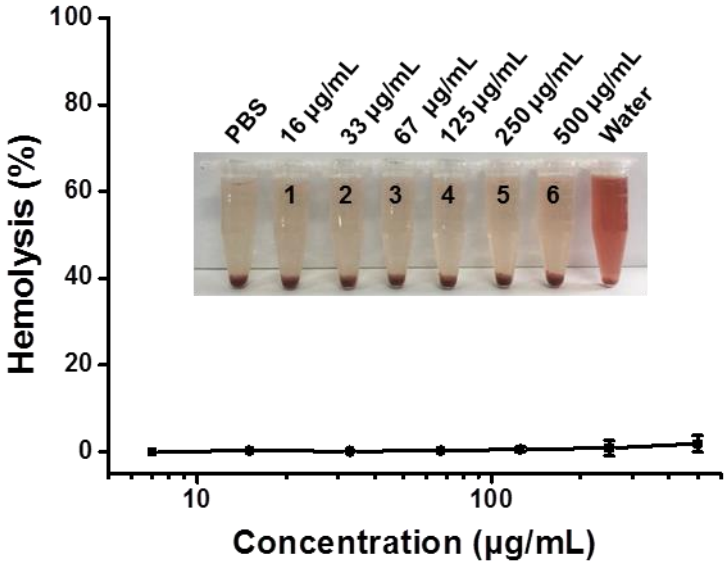

Supplementary Figure 30. Hemolytic analysis of mouse red blood cells after incubation with NTV2. Hemolysis percentage was quantified by measuring the release of hemoglobin into the buffer, and then plotted as a function of the NTV2 concentration. Water was used as a positive control and PBS was used as a negative control. Experiments were performed three times and data were shown as means ± s.d. (n = 3).

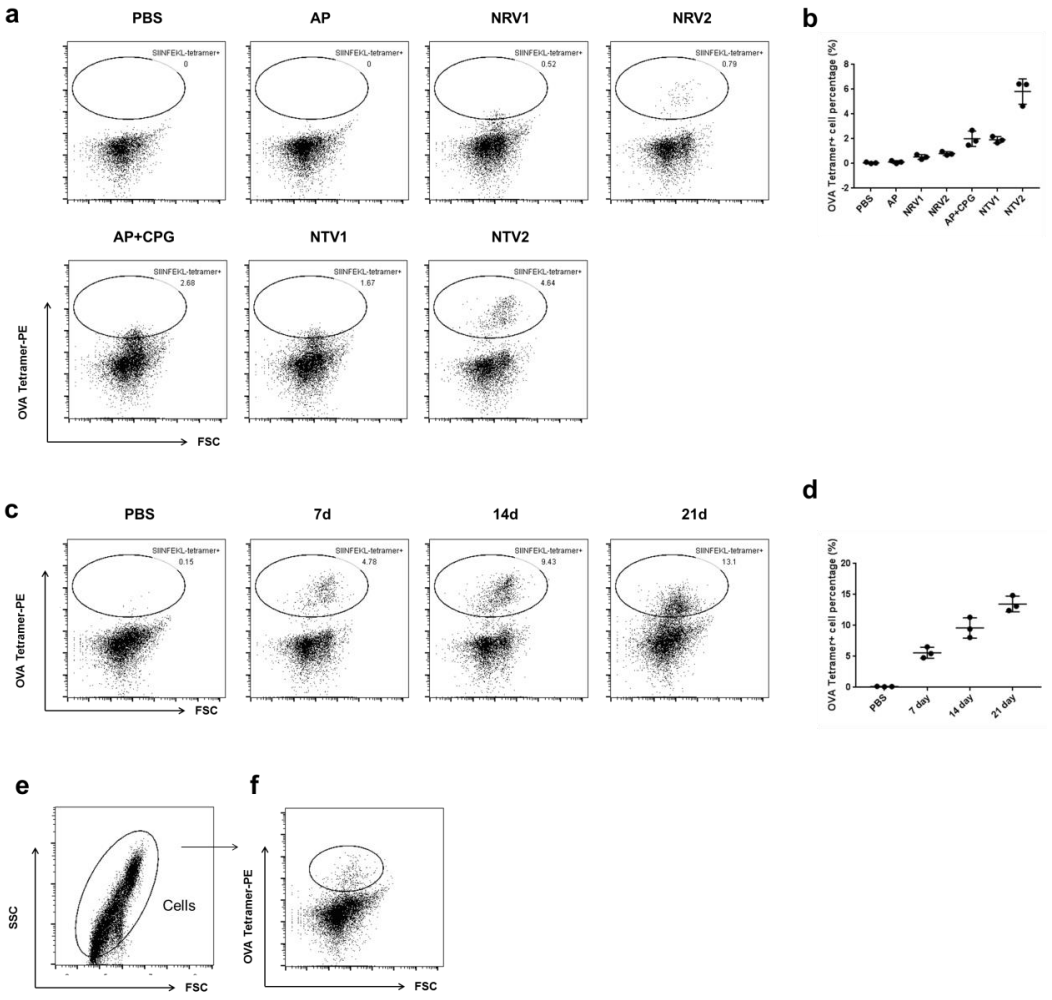

Supplementary Figure 31. Flow-cytometry analysis of the frequency of SIINFEKL-tetramer$^+$ CD8$^+$ T cells in peripheral blood total lymphocytes. Mice were immunized three times at 1-week intervals with free AP (5 μg), a mixture of CPG/AP (5 μg AP and 50 CpG) or NTV2 (125 μg). (**a**) shows the population of SIINFEKL-specific tetramer$^+$ CD8$^+$ T cells in peripheral blood total lymphocytes 24 h after the last immunization with indicated formulations. (**b**) shows the quantification of three independent experiments (n = 3). (**c**) shows the population of SIINFEKL-tetramer$^+$ CD8$^+$ T cells in peripheral blood from NTV2-treated mice after 24 h of the first (day 7)-, second (day 14)-, and third (day 21)-re-stimulation with $OVA_{241-270}$. (**d**), quantification of the SIINFEKL-tetramer$^+$ CD8$^+$ T cell percentage in blood cells. (**e-f**), gating strategy used in the SIINFEKL-tetramer$^+$ CD8$^+$ T cell experiments. Experiments were performed at least three times and data were shown as means ± s.d. (n = 3) in (**b**) and (**d**) from three independent experiments.

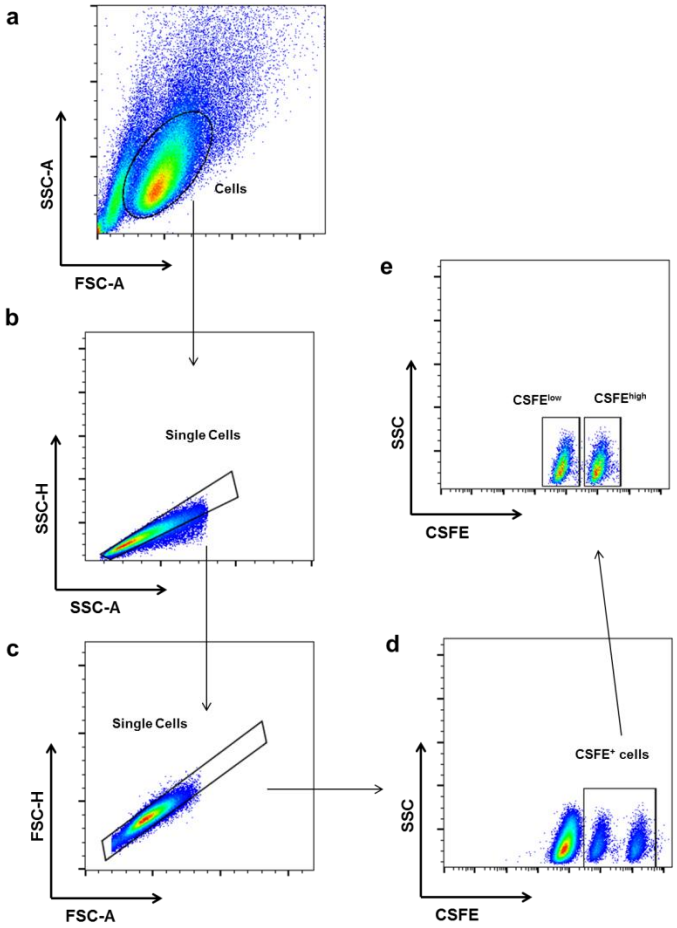

493

494 **Supplementary Figure 32. Gating strategy for *in vivo* killing assay.** Gating strategy for

495 the CSFE-based *in vivo* killing assay, data were presented on Fig 4 g-o.

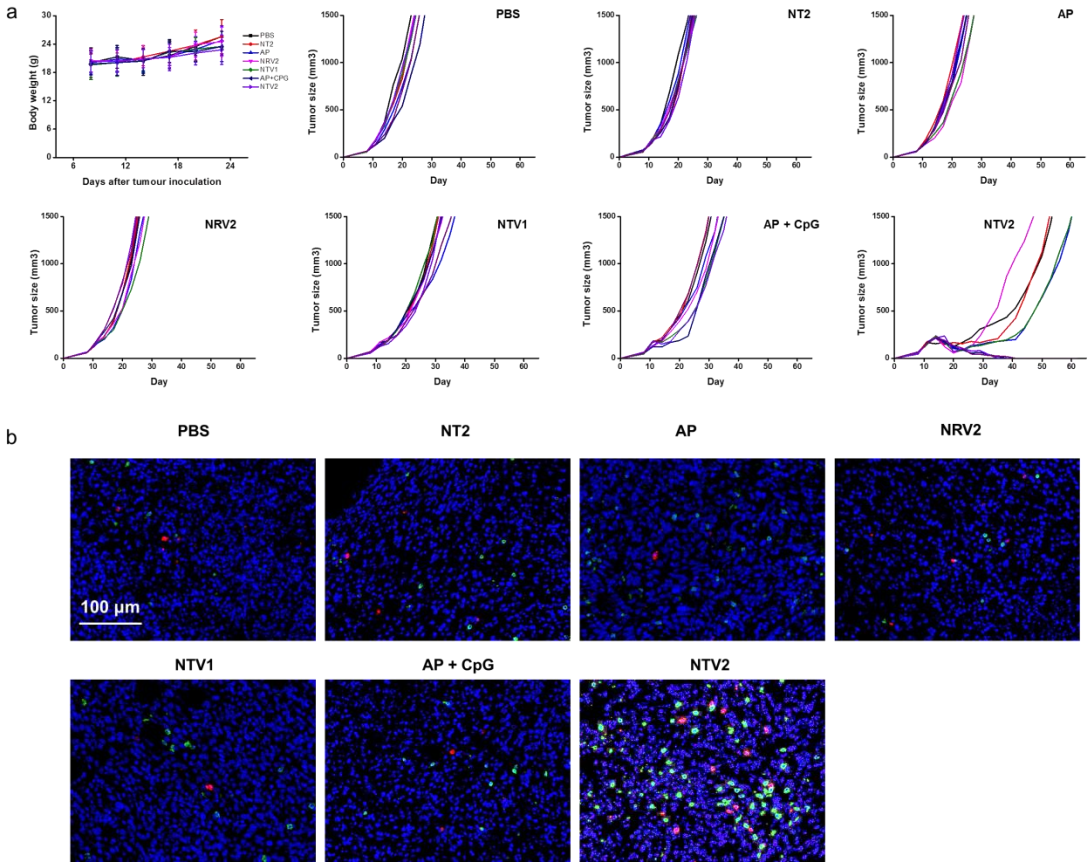

Supplementary Figure 33. Tumour inhibition in B16F10-OVA model. Body weight and individual B16F10-OVA tumour growth curves (n = 8) in mice treated with various formulations are shown in (**a**). Data were shown as means ± s.d. (n = 8) from independent animals. And (**b**), Representative immunofluorescence images of tumours showing $CD8^+$ (green) and $CD4^+$ (red) infiltration in the tumour tissues for all the treatment groups. Scale bar: 100 μm. Experiments were performed for at least three times.

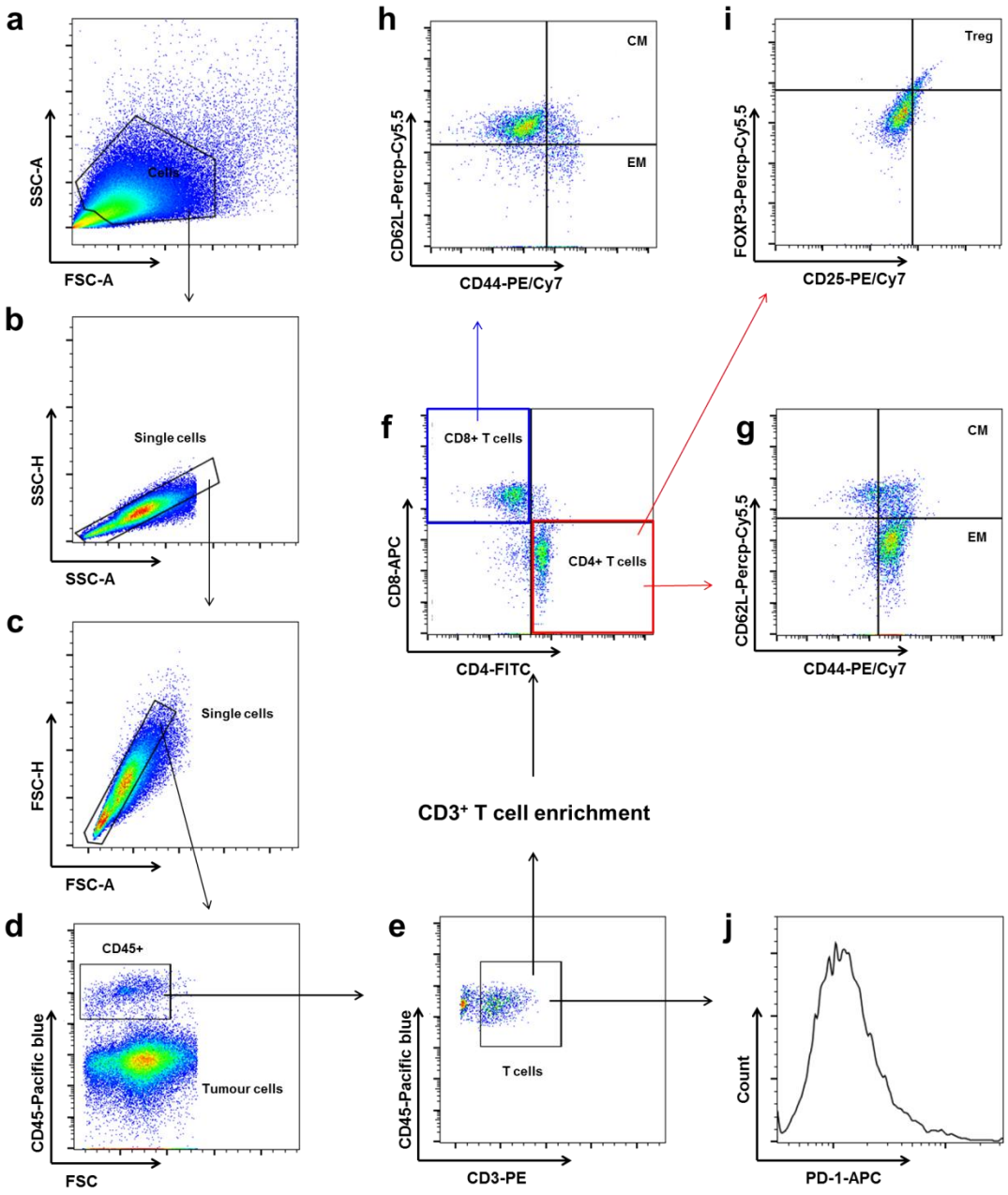

504

505 **Supplementary Figure 34. Gating scheme for flow cytometric analysis of immune**

506 **cell populations in the tumor tissue.** Tumour tissues were treated with collagenase and

507 trypsin to get single cell suspensions and cell aggregates were removed using a 200

508 mesh filter. Gate in (**a**) represents cells, and gates in (**b-c**) represent single cells. Gate in

509 (**d**) shows $CD45^+$ cells. Gate in (**e**) represents $CD45^+CD3^+$ T cells, data were presented

510 on **Fig. 5e, Fig 6f**. Gate in (**f**) represents $CD45^+CD3^+CD4^+$ and $CD45^+CD3^+CD8^+$ T cells,

data were presented on **Fig. 5f**, **Fig 6g**. Gate in (**g**) represents $CD45^+CD3^+CD4^+CD44^+CD62L^+$ central-memory (CM) cells and $CD45^+CD3^+CD4^+CD44^+CD62L^+$ effector-memory (EM) cells in $CD4^+$ T cells, data were presented on **Fig. 5g** and **Fig 6h**. Gate in (**h**) represents $CD45^+CD3^+CD8^+CD44^+CD62L^+$ central-memory (CM) cells and $CD45^+CD3^+CD8^+CD44^+CD62L^+$ effector-memory (EM) cells in $CD8^+$ T cells, data were presented on **Fig. 5h** and **Fig 6i**. Gate in (**i**) represents regulatory T (Treg) cells ($CD45^+CD3^+CD4^+CD25^+FOXP3^+$) in $CD4^+$ T cells, data were presented on **Fig 5i and Fig 6j**. (**j**) Represents the gating method for the PD-1 expression on $CD3^+$ T cells, data were presented on **Fig 5l** and **Fig 6k**.

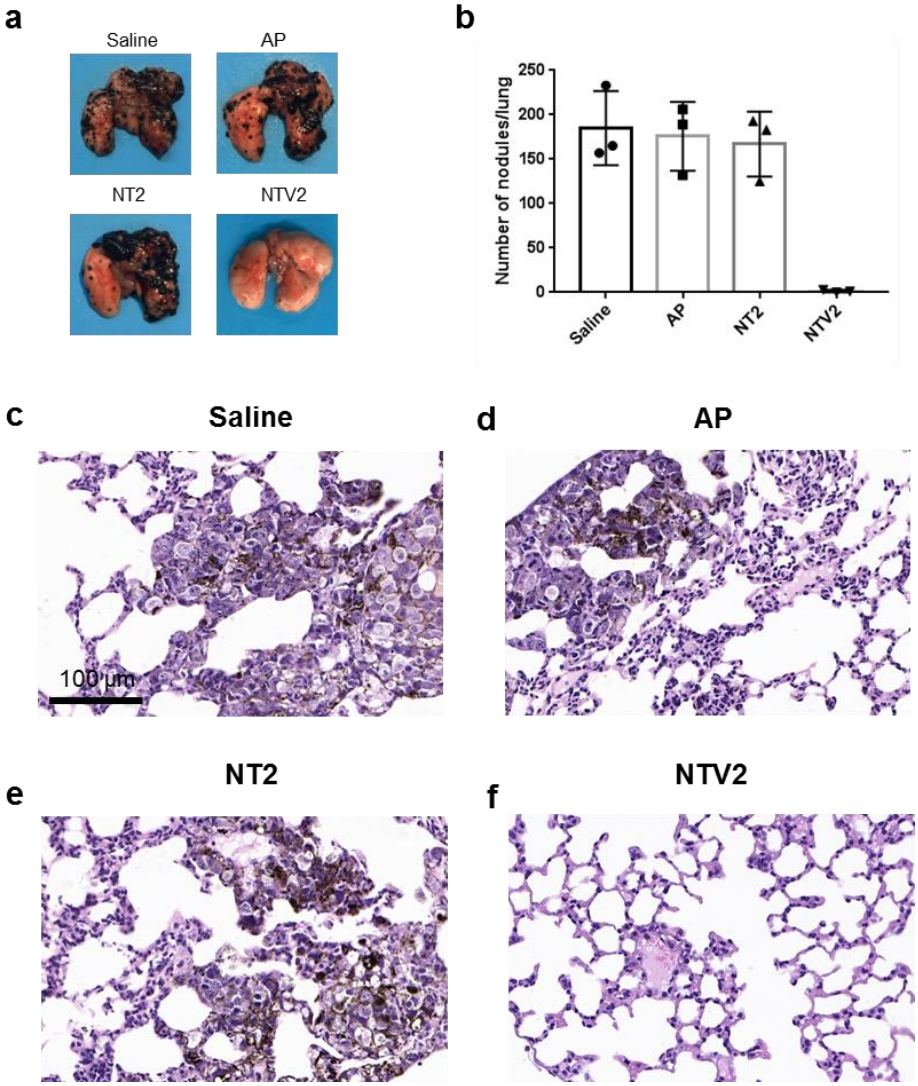

Supplementary Figure 35. nanovaccines prevent cancer challenge. Mice were vaccinated with $OVA_{241-270}$-loaded NTV2 or various nanoparticles for three times (at a 7-days interval). The animals were then i.v. injected with 1×10^5 B16F10-OVA cells at day 7 of the final immunization. After that, mice were killed at day 15 after B16F10-OVA cell injection and the lungs were isolated and representative photographs of the isolated mice lungs (**a**) and average numbers of tumour foci counted in each lung (**b**) (data were shown as mean ± s.d. (n = 3) from three independent animals). (**c-f**), H&E staining of the lungs in different treatment groups. Scale bar: 100 μm. Experiments were performed three times.

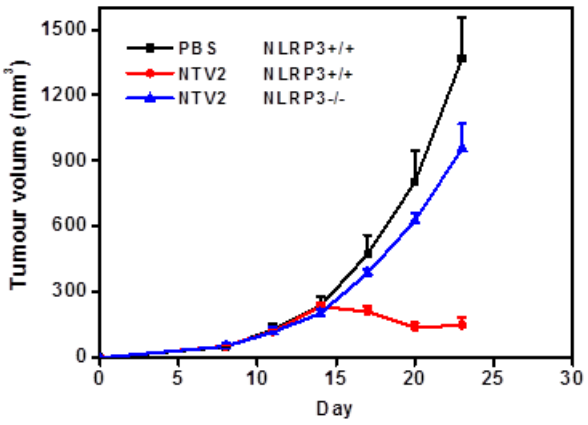

Supplementary Figure 36. Anti-tumor efficiency of NTV2 in NLRP3-/- mice. B16F10-OVA tumor model was constructed by subcutaneous injection of 1×10^6 B16F10-OVA cells to C57BL/6 wild type mouse (NLRP3+/+) or NLRP3 knock-out C57BL/6 mouse (NLRP3-/-). After the tumor volume reach 50 mm^3, NTV2 (loaded with $OVA_{241\text{-}270}$) (AP dose of 5 μg/mouse) was subcutaneously injected to the tail base of the mouse. Injections were given 3 times at 7-day intervals. The tumour volumes were measured every 3 days. Data were shown as means ± s.d. (n = 5) from independent repeats.

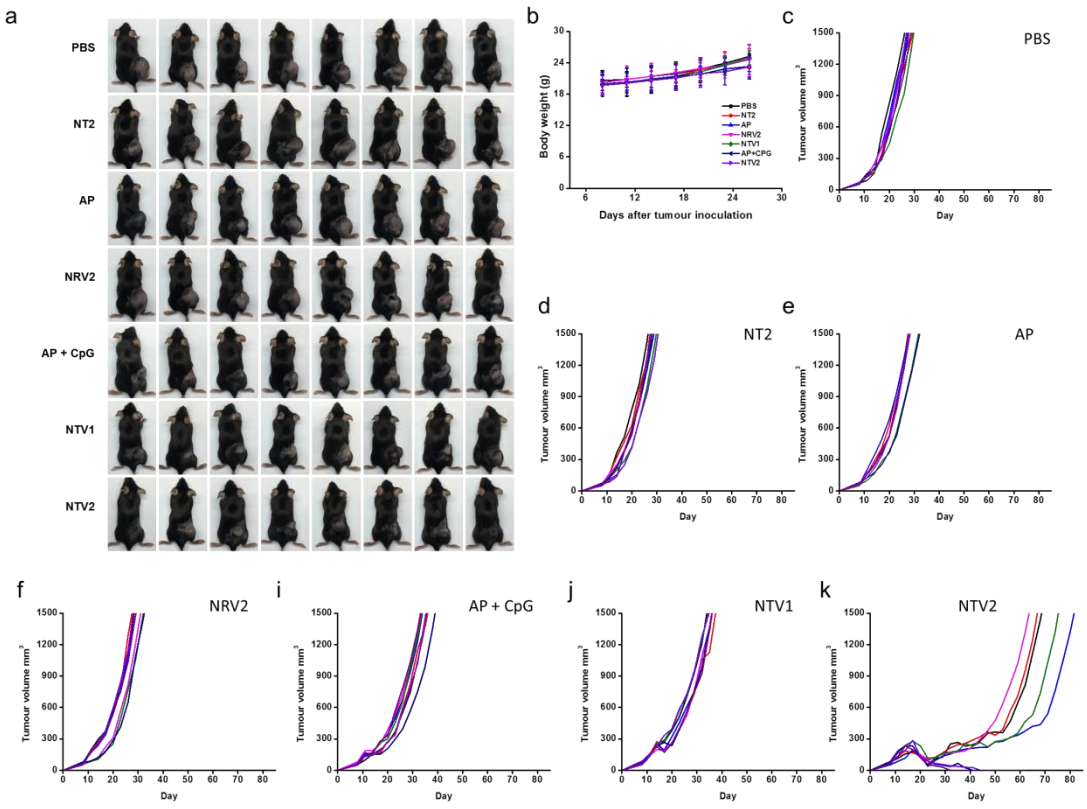

Supplementary Figure 37. NTV has a strong antitumour effect in the HPV tumour model. (**a**), Pictures of mice in different treatment groups at day 26 (n = 8). (**b**), Body weight of mice in different treatment groups (Data were shown as means ± s.d. (n = 8) from independent animals.). And individual TC-1 tumour growth curves in mice treated with various formulations (**c-k**) are shown. Experiments were performed for at least three times.

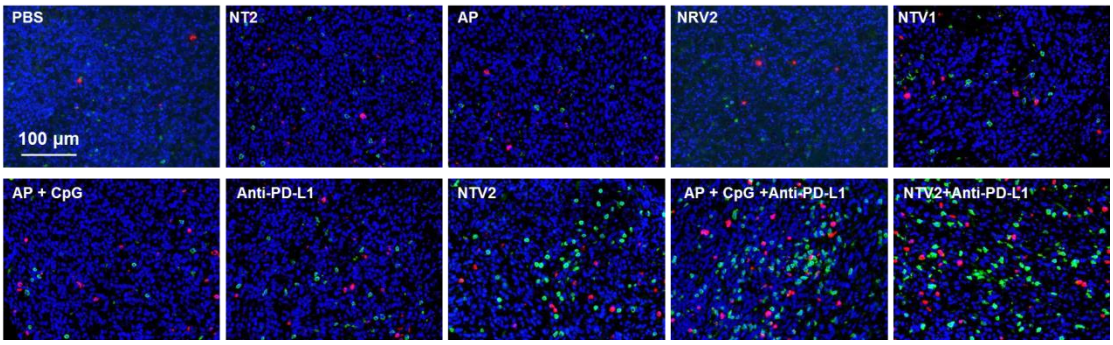

Supplementary Figure 38. T cell infiltration in tumour tissues in the B16F10 tumor model treated with neoantigen vaccines. Representative immunofluorescence images of tumours showing $CD8^+$ (green) and $CD4^+$ (red) infiltration in the tumour tissues for all the treatment groups. Scale bar: 100 μm. Experiments were performed for three times.

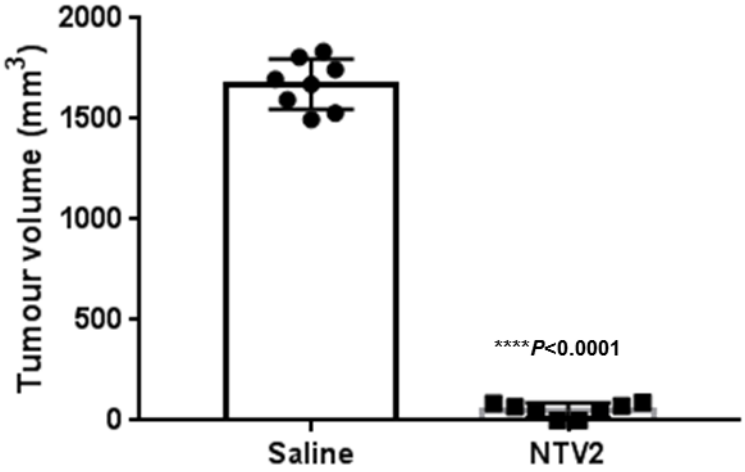

Supplementary Figure 39. Tumour size at 28 days after the tumor-free mice in NTV2 + Anti-PD-L1 group re-challenged with a subcutaneous injection of 10^5 B16F10 cells. C57BL/6 mice were treated three times with NTV2+Anti-PD-L1 (loaded with a mixture of B16-M27，B16-M30，B16-M47，B16-M48) at 7-day intervals. Saline was used as a control. 30 days after the last vaccination, the mice were re-challenged with a subcutaneous injection of 1×10^5 B16F10 cells. 28 days after re-challenging, the tumour volumes from the two groups were measured. Experiments were performed for at least three times. Data are presented as means ± s.d. (n = 8) from independent repeats, analysed by two-tailed unpaired Student's *t*-test, ****$P < 0.0001$.

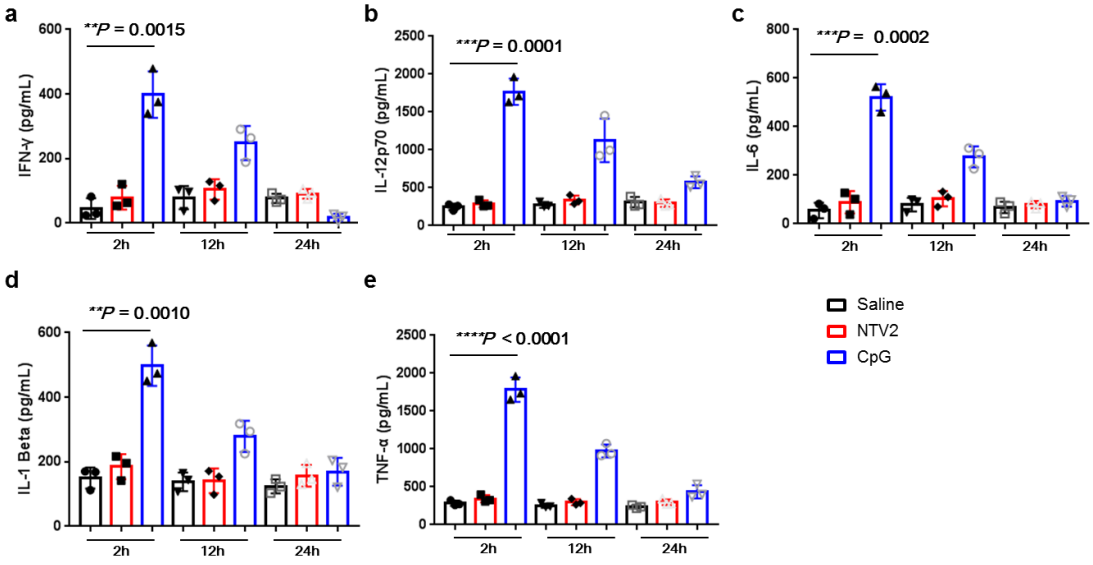

Supplementary Figure 40. Nanovacciens shows limited systemic toxicity *in vivo*. NTV2 induces low systemic levels of cytokines compared with the CpG control. C57BL/6 mice (4 mice per group) were subcutaneously injected with NTV2 (125 μg/mouse) or with 50 μg/mouse CpG. 2 h, 12 h or 24 h after the treatment, serum cytokine levels were measured using ELISA kits for mouse IFN-γ, IL-12p70, IL-6, IL-1β or TNF-α. Three independent experiments were performed, data were presented as means ± s.d. (n = 3), statistical significances were obtained by two-tailed unpaired Student's *t*-test, ****P < 0.0001(**e**), ***P = 0.0001 (**b**), ***P = 0.0002 (**c**), **P = 0.0010 (**d**), **P = 0.0015 (**a**).

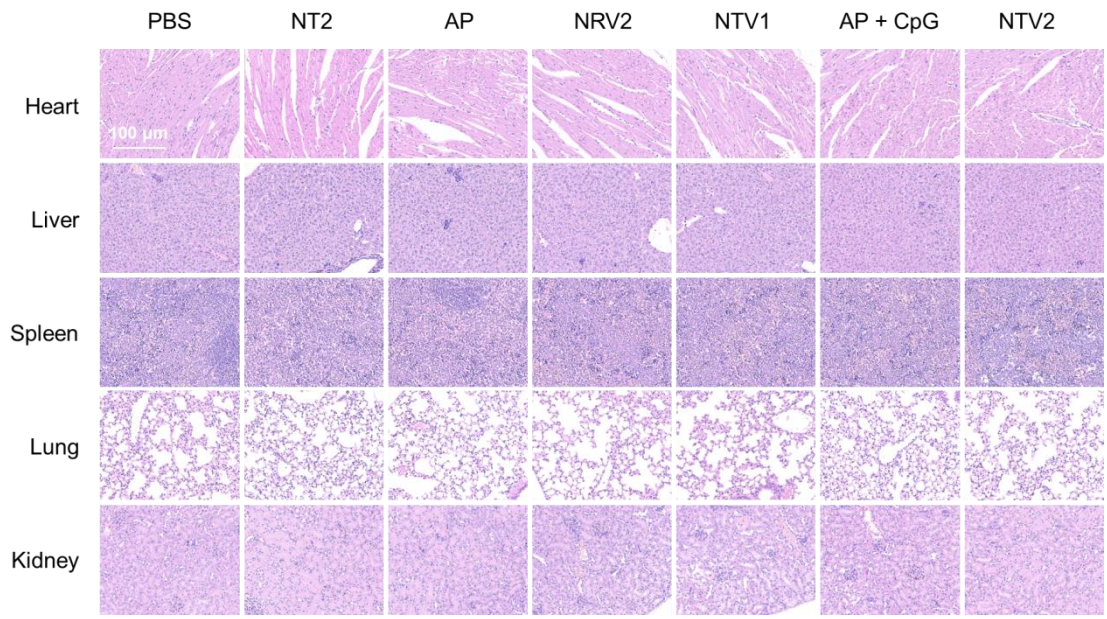

Supplementary Figure 41. Photographs of H&E-stained sections of major organs of B16F10-OVA tumour-bearing miceafter different formulations treatment. Mice were treated with various formulations, and the major organs (heart, liver, spleen, lung, and kidney) were isolated after the mice were killed at day 23. Scale bar: 100 μm. Experiments were performed for at least three times.

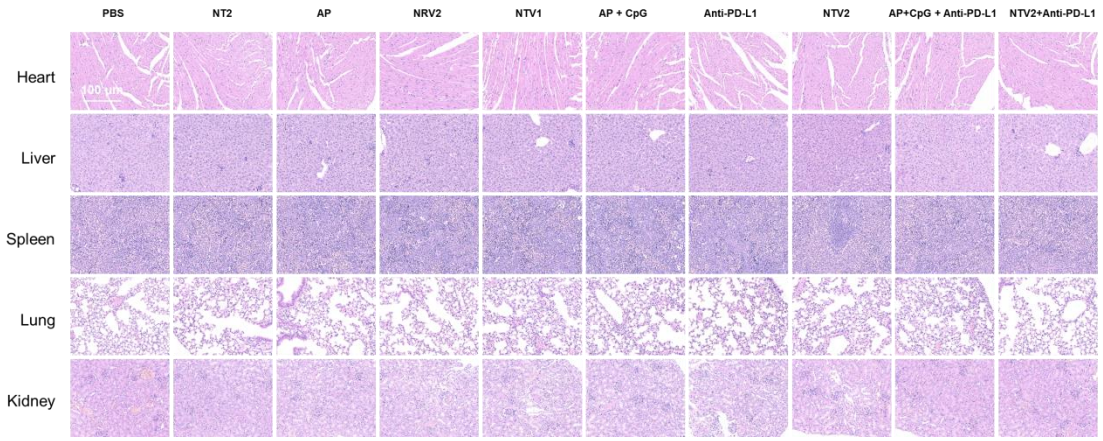

Supplementary Figure 42. H&E-stained sections of major organs of B16F10 tumour-bearing mice after different treatments. Major organs (heart, liver, spleen, lung and kidney) were isolated after the mice were sacrificed at day 26. Scale bar: 100 μm. Experiments were performed for at least three times.

Supplementary Table 1. Characterizations of the fresh synthesized nanoparticles. The size and zeta potential of the fresh synthesized nanoparticles were measured by DLS and the AP loading efficiency in the particles were measured using HPLC. Data were shown as means ± s.d. (n = 3).

NPs	NRV1	NRV2	NTV1	NTV2
Size (nm)	109.3±9.5	98.2±8.3	104.7±9.8	108.6±10.1
Zeta potential (mV)	18.4	17.5	15.7	17.8
AP loading efficiency (%)	3.84	3.59	4.07	4.02

Supplementary Table 2. Characterizations of the nanoparticles. The size and zeta potential of the nanoparticles at day 1, day 5 and day 7 were measured. Data were shown as means ± s.d. (n = 3).

Days	1		5		7	
Nanoparticles	NTV1	NTV2	NTV1	NTV2	NTV1	NTV2
Size (nm)	108.4±9.6	105.3±10.3	103±7.8	104.5±6.9	107±7.9	106.9±7.5
Zeta potential (mV)	15.6	16.5	15.9	14.9	17.4	16.9

Supplementary Table 3. Blood biochemistry analysis. Mice were treated with Saline or NTV2 with different doses and the alanine transaminase (ALT), aspartate transaminase (AST), blood urea nitrogen (BUN) and creatinine (CREA) in mice blood after 7 days of the last NTV2 administration were determined. Data were shown as means ± s.d. (n = 3).

		ALT (U/L)	AST (U/L)	BUN (mM)	CREA (μM)
Saline		111.8±7.5	214.4±12.5	6.7±0.8	42.2±6.7
NTV2	125 μg	98.6±14.5	255±21.3	9.8±1.5	57.3±5.9
	250 μg	87.48±13.2	238.3±35.6	7.3±2.1	48.2±7.9
	500 μg	76.2±21.2	167.6±28.7	5.9±1.7	42.3±4.1
	1000 μg	84.1±15.5	182.4±28.9	6.2±1.5	38.5±3.9
Reference		17-132	54-298	2.8-11.7	18-80